From MRI to Motion: Evaluating Pipelines for Participant-specific Musculoskeletal Modelling in an ACL-Injured Pediatric Population

Elese St Louis, B.Eng.

uOttawa

Master's Thesis

Thesis submitted to the University of Ottawa in partial fulfillment of the requirements for the Master of Applied Science in Biomedical Engineering.

University of Ottawa
Department of Mechanical Engineering
Faculty of Engineering

Supervisor: Dr. Allison Clouthier
Co-supervisor: Dr. Daniel L. Benoit

Thesis Committee:
Dr. Thomas Uchida
Dr. Kawan Rakhra

Acknowledgments

I would like to thank my supervisory team for their support throughout this project. Dr. Allison Clouthier stepped in partway through and brought a level of clarity and organization that helped carry this thesis to completion. I appreciate her responsiveness and steady guidance. Her expertise in musculoskeletal modelling was particularly valuable during the second study, and she was a trusted resource whenever I hit a wall or needed direction. I'm also grateful to Dr. Daniel Benoit, who supervised the early stages of this work – his ability to zoom out and connect research to its broader purpose was invaluable and often helped me reframe challenges along the way. Beyond research, his support during personal obstacles was deeply appreciated and made a lasting impact. I'm also grateful to Dr. Teresa Flaxman, whose expertise in imaging was central to enabling my first study--she made sure I had access to what or who was needed while playing a key role in shaping that project.

To the Clinical Biomechanics Research Lab, thank you for fostering an environment of learning and collaboration. Céline provided early mentorship and helped me find my footing when I first started. Blake, a co-author on my first study, was both a sounding board and steady presence – I appreciate all the chats and shared problem-solving. Karine, your attention to detail and high standards made a lasting impression on how I approach research, from data collection to analysis. You raised the bar and I'm better for it. Zach, although we overlapped briefly, it was nice to have your fresh perspective and to gain your friendship.

To my closest people: Olivia, my best friend and fellow grad student, your support through all of this meant the world, even with the 3,400 km separation. You got it in a way few could. And to my parents--thank you for being there in every way that counted. I couldn't have done this without your quiet backing.

Klappe zu, Affe tot!

General Abstract

Purpose: The development of participant-specific musculoskeletal (MSK) models has the potential to improve the accuracy and clinical relevance of biomechanical simulations. However, while prior research has explored aspects of segmentation and personalization in MSK modelling, the specific trade-offs between segmentation efficiency, anatomical fidelity, and their downstream impact on pediatric knee simulations remain underexplored. This thesis aims to address two key stages in the imaging-to-simulation pipeline for adolescent MSK modelling: (1) evaluating the efficiency and concurrent validity of two segmentation platforms, *MITK* and *Elucis*, and (2) assessing whether incorporating partial participant-specific femur and tibia geometries into *OpenSim* models meaningfully alters simulation outputs during a functional task.

Methods: Study 1 compared segmentation time and agreement between *MITK* (typical, 2D segmentation software) and *Elucis* (3D, virtual reality-based segmentation software) using MRI data from 33 pediatric participants. Inter-rater reliability and inter-software agreement were assessed using Dice Similarity Coefficients (DSC) for the femur, tibia, fibula, and posterior cruciate ligament (PCL) while segmentation time was compared using paired t-tests for the femur, tibia, fibula, anterior cruciate ligament (ACL) and PCL. Study 2 incorporated segmented partial femur and tibia bones into two *OpenSim* models (*Rajagopal* and *Catelli*) using rigid and non-rigid registration (iterative closest point (ICP) and coherent point drift (CPD)) followed by integration via the Shared Tools for Automatic Personalized Lower Extremity Modelling (*STAPLE*) pipeline. Models were scaled using the Automatic Scaling Tool (AST). Model outputs from a forward lunge task were compared across model types using statistical parametric mapping (SPM), and repeated measures ANOVA for three outcomes: knee joint center (KJC) location, knee flexion kinematics, and marker trajectory error.

Results: *Elucis* significantly reduced segmentation time (mean difference = 8.6 minutes; $p < 0.001$) while maintaining comparable or better DSC agreement between raters for the soft-tissue structure (e.g.., PCL; inter-rater DSC = 0.77 in *Elucis* vs. 0.57 in *MITK*). Femur, tibia, and fibula DSC scores remained high across both platforms (inter-software) and between raters (inter-rater; DSC $\geq$ 0.90). In MSK simulations, partial bone personalization led to inconsequential changes in KJC (< 0.006 mm) and non-significant differences in knee flexion waveforms ($p > 0.05$). Only one model comparison (Participant-specific *Catelli* vs. Generic *Catelli*) showed a statistically significant difference in marker root mean square (RMS) error ($p < 0.001$), but the absolute difference remained below 0.25 mm, far under biomechanical relevance thresholds.

Conclusion: This thesis demonstrates that *Elucis* offers a time-efficient alternative to traditional segmentation platforms, particularly for challenging soft-tissue structures like the PCL. However, incorporating partial participant-specific geometry alone did not substantially alter kinematic or marker-based outputs during a controlled functional task of the forward lunge. These findings highlight the importance of aligning the degree and type of model personalization with the specific research or clinical application. Full anatomical personalization or more complex movement tasks may be required to detect meaningful difference in simulation outcomes.

List of Abbreviations

ACL	Anterior cruciate ligament
ANOVA	Analysis of variance
AST	Automatic scaling tool
BW	Body weight
CPD	Coherent point drift
DOF	Degrees of freedom
DSC	Dice similarity coefficient
EMG	Electromyography
GRRAS	Guideline for reporting reliability and agreement studies
ICP	Iterative closest point
IK	Inverse kinematics
KJC	Knee joint center
LCL	Lateral collateral ligament
MAP	Musculoskeletal atlas project
MCL	Medial collateral ligament
MITK	Medical imaging interaction toolkit
MRI	Medical resonance imaging
MSK	Musculoskeletal modelling
MTU	Musculotendon unit
PCA	Principal component analysis
PCL	Posterior cruciate ligament
RMS	Root mean square
RMSE	Root mean squared error
SPM	Statistical parametric mapping
SSMs	Statistical shape models
STAPLE	Shared tools for automatic personalized lower extremity modelling

Co – Authorship

This thesis includes two un-published manuscripts. The authorship is as follows:

Chapter 2: Study 1 – "3D Modelling from MRI of pediatric knees using virtual reality and segmentation platforms: An inter-rater and inter-software comparison"

Elese St Louis, Blake Miller, Allison Clouthier, Daniel L. Benoit, Sasha Carsen, and Teresa Flaxman

Author Contributions: Conceptualization, E.S., D.B., and T.F.; methodology, E.S., B.M.; software, E.S., B.M., and T.F.; validation, E.S., T.F.; formal analysis, E.S.; investigation, E.S., B.M.; resources, D.B., S.C., and T.F.; data curation, E.S., and B.M.; writing—original draft preparation, E.S.; writing—review and editing, E.S., A.C., D.B., B.M., and T.F.; visualization, E.S..; supervision, D.B., T.F., and A.C.

Chapter 3: Study 2 – "MRI-based Participant-specific vs. Generic Musculoskeletal Models: Effects on Marker Fit, Flexion Kinematics, and Participant-Level Patterns"

Elese St Louis, Allison Clouthier, Karine Stoelben, Sasha Carsen, and Daniel L. Benoit

Author Contributions: Conceptualization, E.S., D.B., and A.C.; methodology, E.S., A.C.; software, E.S., and A.C.; validation, E.S.; formal analysis, E.S. and A.C.; investigation, E.S., K.S. and A.C..; resources, D.B., S.C., and A.C.; data curation, E.S.; writing—original draft preparation, E.S.; writing—review and editing, E.S., A.C., K.S., and D.B.; visualization, E.S.; supervision, A.C., D.B.

Table of Contents

Chapter 1: General Introduction/Background

1.1 Thesis Scope

The human knee joint plays a central role in supporting bodyweight and enabling dynamic movement (Vaienti et al., 2017, Weiss et al., 2001, Pinskerova et al., 2020). In recent years, computational models of the musculoskeletal (MSK) system have been increasingly used to simulate joint mechanics and muscle forces during movement. These models offer non-invasive insights into internal tissue loading and joint behaviour, which are otherwise difficult or unethical to measure in vivo (Conconi et al., 2018).

This thesis focuses on two key challenges in participant-specific MSK modelling of the knee: (1) evaluating the segmentation efficiency and agreement between two software platforms (*MITK* v. *Elucis*) for producing 3D knee geometries from MRI data, and (2) assessing how the use of personalized bone geometries affects *OpenSim* simulation outputs compared to generic models.

The data for this study are sourced from an ongoing, longitudinal study investigating ACL injuries in adolescents. This thesis contributes to the methods used to analyze this dataset, focusing on accessibility, reliability, and meaningfulness of using MRI data to enhance downstream knee joint biomechanics modelling workflows.

1.2 The Knee Joint: Anatomy and Function

1.2.1 Overview of the Knee

The knee is a compound synovial joint composed of the tibiofemoral and patellofemoral joints (Gupton et al., 2022, Vaienti et al., 2017) (Figure 1.1.1). It allows for six degrees of freedom (DOF), including flexion-extension, internal-external rotation, varus-valgus, anterior-posterior translation, medial-lateral translation, and compression-distraction (Benoit et al., 2007). While flexion-extension is often considered the primary functional motion during daily and athletic activities, it does not occur in isolation (Vaienti et al., 2017, Weiss et al., 2001).

In vivo imaging has shown that functional flexion is accompanied by coupled tibial axial rotation and anterior-posterior translation to maintain joint congruency between the femoral condyles and the tibial plateau (Smith et al., 2021; Li et al., 2005). Conconi et al. (2023), using dynamic MRI during a closed chain squat task, observed tibial internal rotation and posterior translation relative to the femur which highlights the multiplanar motion of the tibiofemoral joint even in functional tasks.

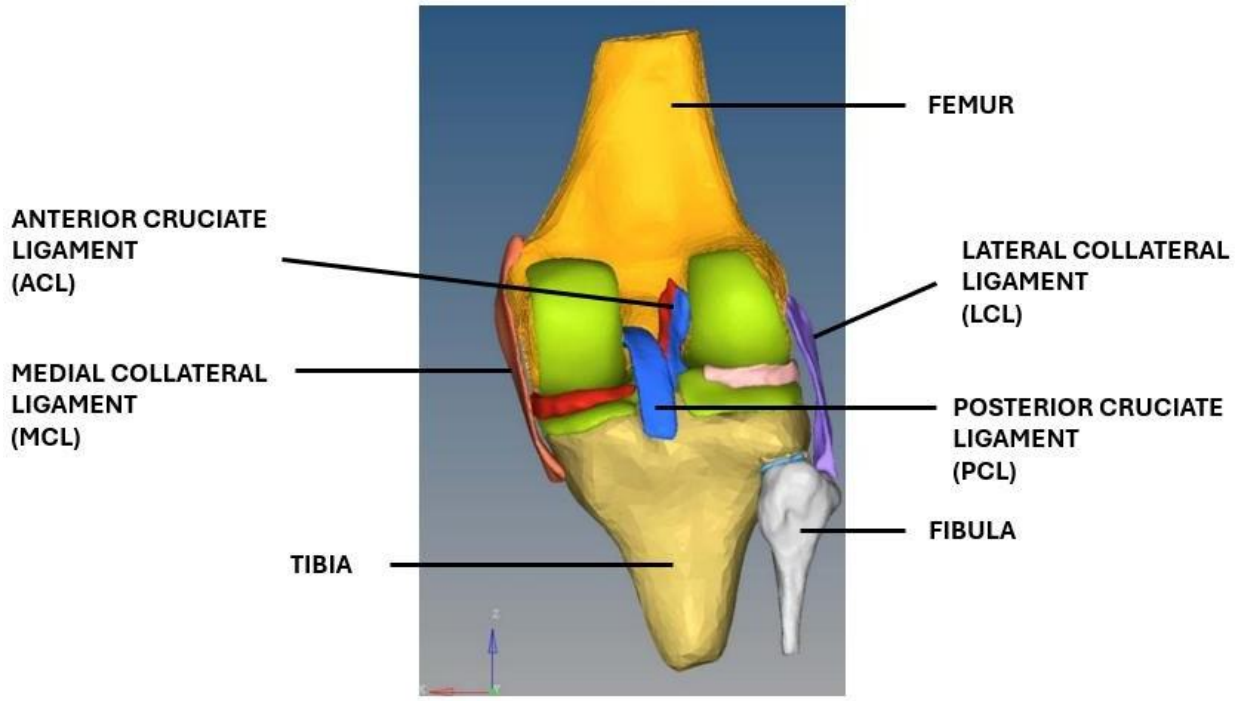

Figure 1.1: Posterior view of the knee joint comprising the long bones, (femur, tibia, and fibula) with the four main ligaments, (anterior cruciate ligament (ACL), medial collateral ligament (MCL), posterior cruciate ligament (PCL), and lateral collateral ligament (LCL)) (Yang, 2020)

Passive knee stability is primarily maintained by four key ligaments: the anterior cruciate ligament (ACL), posterior cruciate ligament (PCL), medial collateral ligament (MCL), and lateral collateral ligament (LCL) (Weiss et al., 2001) (Table 1.1). These ligaments constrain excessive movement, aid in load transmission, and support dynamic stabilization of the joint (Woo et al., 2006). In vivo studies confirm that the ACL resists anterior tibial translation and internal rotation, particularly in early flexion, while the PCL develops greater strain with increasing flexion (Li et al., 2005; D' Lima et al., 2007). More structures that contribute to passive knee stability include the joint capsule and the retinacular tissues, particularly the medial and lateral patellar retinacula, which resist excessive patellar translation during flexion-extension and stabilize patella tracking (Nomura et al., 2005), while the posterior capsule and associated ligaments provide support to posterior joint integrity (LaPrade et al., 2007). These accurate characterizations of knee kinematics require high-fidelity measurements. The motion of the patella within the femoral trochlea and the rolling-gliding behaviour of the femoral condyles on the tibial plateau contribute to complex internal dynamics (Pinskerova et al., 2020). Studies show that using bone-pin and fluoroscopic tracking have revealed that traditional skin-based marker systems may oversimplify or distort these internal joint mechanics (Benoit et al., 2006; Smith et al., 2021; Conconi et al., 2023).

Table 1.1: Ligaments and their functions in the knee (Neumann, 2001, Masouros et al., 2010, Weiss et al., 2001)

Structure	Function
Anterior Cruciate Ligament	• Resists excessive anterior tibial translation and posterior femur translation • Limits full knee extension • Resists extreme varus, valgus, and axial rotation
Posterior Cruciate Ligament	• Resists excessive posterior tibia translation and anterior femur translation • Most fibers become taut at full flexion • Some fibers are taut at maximal hyperextension and extreme ends of varus, valgus, and axial rotation
Lateral Collateral Ligament	• Resists varus, knee extension, and axial rotation
Medial Collateral Ligament	• Resists valgus, excessive knee extension, and axial rotation

Finally, the knee also plays an important proprioceptive role. Mechanoreceptors, in structures such as the cruciate ligaments and the joint capsule of retinacular tissues, contribute to neuromuscular feedback loops that coordinate muscle control and protect the joint under dynamic conditions (Krogsgaard et al., 2011; Cabuk et al., 2016; Zimny et al., 1991).

1.2.2 ACL Injuries in Adolescents

While this thesis does not directly examine injury mechanisms, it uses data from a larger clinical study focused on anterior cruciate ligament (ACL) injuries in adolescents. In this population, ACL ruptures are one of the most common ligamentous injuries (Bradsell et al., 2022). The ACL plays a vital role in resisting anterior tibial translation, accounting for approximately 86% of the passive restraint (i.e., in the absence of muscle activation), as well as limiting the varus-valgus stress and providing mechanosensory feedback to the quadriceps (Escamilla et al., 2012, Ohori et al., 2017, Konishi et al., 2002).

In individuals with an ACL rupture, altered loading patterns and disrupted sensory input can lead to compensatory strain on the other knee structures and potential long-term adaptations (Krogsgaard et al., 2011). While this pathophysiological context is not the focus of the present work, it is relevant as the anatomical variability post-injury, including joint center shifts or bone geometry changes, may influence the joint modelling outcomes. Therefore, understanding the structural and functional role of the ACL provides useful context for interpreting knee-specific MSK simulations.

1.3 *OpenSim* Simulation Framework

OpenSim is an open-source software platform used to build, visualize, and simulate musculoskeletal (MSK) models of human and animal movement. It enables researchers to estimate internal biomechanics, such as joint angles, muscle forces, and joint loads, based on motion capture or other input data. While several platforms exist for MSK modelling, including *OpenSim* and *AnyBody*, direct comparison is complicated by differences in modelling assumptions and joint definitions (Kim et al., 2018). *OpenSim* was selected for this study due to its open-source accessibility, strong community support, and widespread adoption in gait and pediatric biomechanics (Seth et al., 2018). This section outlines key procedures involved in using *OpenSim* for MSK simulation, including model selection, scaling, inverse kinematics, and evaluation of marker error.

1.3.1 Overview

Musculoskeletal (MSK) models simulate the internal mechanics of human movement and while the foundational components of these models, such as rigid bodies, mobilizers, actuators, and contact elements, are shared across frameworks, specific design choices vary considerably depending on intended application and population. The choice of MSK model is a critical step in simulation design as it influences the assumptions and constraints of simulation outputs.

Several generic models have been developed in *OpenSim*, and each offering different levels of anatomical detail and computational complexity. Among the earliest are Gait2392 and Gait2354 models, which were originally designed to analyze gait and feature 23 degrees of freedom (DOF) with 92 or 54 musculotendon actuators, respectively (Delp et al, 2007, Thelen et al, 2003). These models use simplified joint definitions and generic musculature to allow for efficient simulation of common gait tasks which make them popular for demonstration purposes; however, for higher-flexion tasks, the models pose limited suitability.

In contrast, the *Rajagopal* et al. (2016) model was created to improve simulation accuracy for healthy, young adults, building directly upon the foundational lower-limb structure of the Arnold et al. (2010) model. While *Arnold*'s model was based on cadaveric data from older adults, *Rajagopal* incorporated MRI-based muscle volume data from young individuals (Handsfield et al., 2014). The *Rajagopal* model includes 22 rigid bodies, with 20 lower-limb DOFs and 80 Hill-type musculotendon actuators. The knee joint model itself is modelled with a one-DOF flexion-extension knee joint, constrained to a maximum of 120°, with other rotational and translational DOFs constrained through spline functions tied to knee flexion. *Rajagopal* has become a widely adopted baseline for research focused on lower-limb joint mechanics (Smale et al., 2019, Miller et al., 2023).

The *Catelli* et al. (2019) model builds on the work of Lai et al. (2017) who extended the *Rajagopal* model to support high-flexion tasks by modifying muscle-tendon parameters and paths. *Catelli* et al. (2019) and refined the coupled translational behaviour of the tibia relative to the femur based on data from Buford et al. (1997). These translational modifications primarily affect knee behaviour beyond 60° of flexion but do not alter the primary flexion-extension rotation, which remains modelled as a single-DOF joint. Catelli et al. (2019) further refined muscle paths and wrapping surfaces to enable knee flexion up to ~ 145° which enhances simulation fidelity for deep squats and other high-ROM tasks. The structural consistency, despite differences in joint parameter limits, enables controlled comparisons of musculoskeletal outputs, particularly when evaluating the impact of participant-specific bone geometries.

1.3.2 Scaling in *OpenSim*

Accurate scaling of *OpenSim* MSK models is critical to ensure that body dimensions, mass distributions, and marker positions reflect participant-specific anatomy. Scaling is typically completed by comparing the positions of model markers on the unscaled model to experimental markers collected during a static calibration trial. Scale factors are computed for each model segment based on distances between pre-determined marker pairs to adjust segment proportions, mass properties, and joint axes. This process works to align the generic MSK model to a participant's anthropometry and is a necessary step prior to running simulations for meaningful and accurate analysis.

Scaling can be performed on segments through uniform or non-uniform methods. Uniform scaling assumes isotropic changes across all axes and is generally more robust when medical imaging is unavailable, while non-uniform scaling allows more anatomical flexibility (Anderson et al., 2021). Essentially, uniform scaling preserves the anatomical proportions of model elements and avoids introducing geometric distortions; however, it cannot accommodate participant-specific differences in bone shape or segment proportions that deviate from the generic model (Lund et al., 2015). Like MSK model selection, it is hard to support one form of scaling over another, as the intended use of the model will dictate the most appropriate method of scaling the model.

1.3.3 The Automatic Scaling Tool (AST)

The Automatic Scaling Tool (AST) was developed to enhance the standard scaling procedure for *OpenSim*. Rather than relying solely on static measurements or manually defined scale factors, AST iteratively adjusts body segments and model marker positions to minimize the error between experimental and model marker positions while preserving anatomical relationships across connected segments (Di Pietro et al., 2023). Essentially, AST locates the maximum marker error present after each iterative attempt at scaling, and works through that marker's placement, or the segment present to improve the marker error with a pre-determined AST pipeline adjustment factor. At each iteration, marker placement, joint axes, and mass properties are updated to maintain dynamic and anatomical consistency across the model (Di Pietro et al., 2023). This structured process improves the reproducibility of model scaling compared to conventional manual scaling methods, which rely heavily on user-defined decisions and may introduce variability across participants (Di Pietro et al., 2023).

1.3.4 Inverse Kinematics in *OpenSim*

Inverse kinematics (IK) is a computational approach used to estimate joint angles and segment poses based on observed motion data from a motion capture system. In biomechanical applications, IK begins in the global laboratory coordinate system of the motion capture system, and marker trajectories are transformed through a series of reference frames to define joint coordinate systems (Uchida et al., 2021). From these relationships, joint angles can be computed based on relative motion between adjacent anatomical frames across time.

OpenSim solves IK using a frame-by-frame weighted least squares optimization. At each frame, it minimizes the sum of squared distances between experimental markers and their corresponding model markers. During this process, *OpenSim*'s IK solution is constrained, thereby enforcing rigid body assumptions of the models as well as joint connectivity throughout the simulation. These constraints simplify the optimization problem but may limit physiological realism, particularly at joints like the knee where multiple DOFs are known to exist (Benoit et al., 2007; Smale et al., 2019). As such the model does not replicate in vivo joint kinematics directly

but rather offers a solution to estimating generalized motion within a constrained biomechanical framework.

1.3.5 Marker Error

Marker error refers to the discrepancy between the positions of experimental markers collected during motion capture and the corresponding model markers on the MSK models. In *OpenSim*, this error is calculated during inverse kinematics as the residual distance between the experimental and model marker sets and can be reported as (1) root mean square (RMS) error, (2) maximal error, or (3) total squared error. RMS error is the square root of the average squared distance between each experimental marker and corresponding model marker across all frames of the trial. Maximal error is the largest single marker error observed during the entire trial to highlight the worse discrepancy between any pair of experimental and model markers. Total squared error is the sum of the squared distances between experimental and model markers across all markers and frames, but it is sensitive to trial length and number of markers. A lower marker error indicates better fit between the model and the observed motion, while higher errors can signal misalignment in scaling, marker placement, or joint definitions. *OpenSim*'s best practice suggests that marker tracking errors should remain below 20 mm to maintain biomechanical validity (*OpenSim* Team, 2019). Marker error alone does not guarantee model accuracy, but it does serve as an important quality check within simulations.

Sources of marker error can arise at several stages of the motion capture and modelling workflow. First, marker placement error arises from variation in locating anatomical landmarks across evaluators, even with training and standardized protocols, and can result in frame-to-frame inconsistencies (Malus et al., 2021). Second, soft tissue artifact (STA) results from movement of skin and muscle relative to the underlying bone during motion causing the physical marker to deviate from the assumed rigid segment motion, which has been quantitatively characterized during dynamic tasks by Leardini et al. (2005). Third, errors can happen during inverse kinematics (IK) optimization in *OpenSim*. Although experimental marker trajectories captured in the systems like *VICON* are accurate to sub-millimeter levels, *OpenSim* computes model kinematics by minimizing the distance between these experimental markers and the model's virtual markers. Any deviation introduced represents a modelling artifact, not experimental noise, and even a 2 cm mismatch can cause joint angle errors exceeding 15° in some cases (Uchida et al., 2022). Improper registration or weighting of markers during scaling and IK can exacerbate these discrepancies (Schellenberg et al., 2017). Ultimately, it is essential to distinguish these error sources when evaluating model accuracy and interpreting results.

1.4 Personalization of Musculoskeletal Models

1.4.1 Importance of Patient-Specific Modelling in Biomechanics

MSK models are computational tools designed to represent human movement by simulating the interaction of bone, joints, ligaments, and other soft tissues. These models typically include rigid bodies (bones), mobilizers and constraints (joints), contact elements (to simulate ground reaction forces), and force-generating actuators (muscles and ligaments) (Seth et al., 2011). The development of MSK models is often based on data from specific populations, either due to accessibility or research interest. For example, some models are built on cadaveric data, where bone geometries are derived from elderly male donors, such as those in the creation of the Arnold et al. (2010) model. Others focus on simulating age-specific musculoskeletal properties; for

instance, the Thelen et al. (2003) model was developed to represent age-related muscle force-velocity characteristics in older adults. In contrast, the *Rajagopal* et al. (2016) model was designed using muscle volume data from a young, healthy population (Handsfield et al., 2014), and the *Catelli* et al. (2019) model further refined joint definitions to better simulate large flexion angles in dynamic tasks common among youth populations.

However, generic MSK models from these specific datasets may not accurately represent the anatomical or functional characteristics of different populations in their entirety. This mismatched data can lead to inaccuracies in joint center estimation, segment mass distribution, or muscle path geometry which impacts simulation outputs, such as joint angles or moments (Delp & Maloney, 1993). Personalized MSK models help address this issue by allowing the researcher to retain the validated framework of the generic model while replacing specific pieces of the whole model with personalized components, for example bone geometries or joint definitions. This enables models to better capture anatomical variability or pathology-specific changes from participants to improve the accuracy and physiological relevance of the simulation outputs, such as moment arm lengths or joint loads (Scheys et al., 2008, Modenese et al., 2018).

1.4.2 Levels of Personalization in Musculoskeletal Models

Musculoskeletal (MSK) models can be personalized at multiple levels to better represent participant-specific anatomy and physiology. The choice and extent of personalization depends on the goals of the study, available data, and the computational cost of implementation. Personalization can occur at the level of bones, muscles, ligaments, or joint constraints and can be applied in isolation or in combination, and each scenario has unique implications for simulation fidelity and output sensitivity.

1.4.2.1 Bone Personalization

A commonly explored personalization approach involves updating bone geometries to reflect participant-specific anatomy. Prior studies have used a variety of approaches in bone personalization, like only replacing a single bone, multiple bones, or full lower limbs to investigate geometry impacts on simulation outcomes. Martelli et al. (2015) found that for tibiofemoral geometry, replacing the tibia and femur with participant-specific geometry significantly affected knee kinematics, while later work (Martelli et al., 2020) showed it determines tibiofemoral motion during walking with substantial force differences observed in specific individuals.

In pediatric modelling, Kainz et al. (2021) demonstrated that femoral geometry, particularly neck-shaft angle and anteversion, alters hip joint contact forces and growth predictions. Davico et al. (2020) extended this work by evaluating ten pipelines for reconstructing pediatric bones using the Musculoskeletal Atlas Project (*MAP*) Client, a software tool for reconstructing pediatric bone geometries. MRI-informed pipelines were most accurate in this study, especially for hip joint center estimation, while a linearly scaled generic *OpenSim* model alone performed poorly, especially in a pediatric population (Davico et al., 2020).

The influence of bone morphology extends beyond kinematics as well. Charles et al. (2021) used dynamic biplane radiography and participant-specific models to predict ACL forces during walking. From this investigation, ACL force predications from personalized models were compared to those from scaled generic models, with root mean squared (RMS) differences reaching up to 0.27 bodyweights (BW). The personalized models incorporated subject-specific joint geometry and ligament parameters.

These studies confirm that participant-specific bone geometries impact joint mechanics, soft-tissue loading, and simulation accuracy. However, most of these studies combine bone

personalization with changes to muscles or ligaments beyond re-mapping to the new participant-specific bones. An exploration into the isolated effect of bone on geometry alone, especially in pediatrics, would show if bone personalization is sufficient to alter simulation outcomes, and if so, to what degree.

1.4.2.2 Muscle Personalization

Muscle definition in MSK models can be personalized by adjusting path points, force-generating parameters, and activation strategies to better reflect participant-specific anatomy and function. A common approach involves morphing muscle paths based on changes in bone geometry (Modenese et al., 2021) or directly extracting origin and insertion sites from medical images when available (Killen et al., 2021). These adjustments improve the biofidelity of muscle-tendon unit kinematics and reduce instances of unrealistic path penetrations (e.g., through surrounding structures).

Studies have also explored these strategies in pediatric and clinical populations. Van Den Bosch et al. (2022) demonstrated that incorporating MRI-informed MSK geometry into simulations of a child with cerebral palsy had the largest influence on gait deficits, more than muscle strength adjustments or length of muscles. Similarly, Davico et al. (2022) implemented a multi-level personalization pipeline, including image-based anatomy, electromyography (EMG) informed activation, and tuned musculotendon unit (MTU) parameters, which yielded physiologically plausible joint contact force predictions in children with and without cerebral palsy. Despite these findings, muscle personalization in pediatric populations remains constrained by practical challenges, yet with emerging optimization frameworks and imaging techniques, accurate, participant-specific muscle definitions are becoming increasingly feasible (Xu et al., 2025).

1.4.2.3 Ligament Personalization

Ligament structures can be personalized, but this introduces challenges in image segmentation and material property estimation from imaging. Smale et al. (2019) addressed the absence of knee ligaments in the *Rajagopal* model by using MRI-based point clouds to identify participant-specific origins and insertions of ligaments in the tibiofemoral joint. In Smale et al.'s (2019) study, the MRI-personalized model produced significantly different knee kinematics and ligament elongation patterns compared to generic models which produced increased knee abductions and more physiological ligament strains during cutting tasks. Another example of ligament personalization is with Marieswaren et al. (2018) who extended *OpenSim* to incorporate 25 ligament and capsule bundles with elastic properties informed by MRI. The simulations revealed that specific motions, such as knee adduction and rotation, generated strain levels approaching or exceeding known failure thresholds, emphasizing the role of model personalization in injury-risk predictions. These studies showed that MSK models respond to origin-insertion locations, and tissue-specific mechanical parameters.

1.4.2.4 Joint Definition

Joint definitions directly impact model fidelity and simulation outcomes, but it is possible to personalize them. Simplified representations, such as the one-DOF knee in the *Rajagopal* model, restrict all motion to be spline-interpolated functions of the flexion-extension angle, which fails to account for secondary translations or rotations. Miller et al. (2023) addressed this by combining high-resolution bone geometries with literature-derived fluoroscopic data to partially unlock the knee's remaining DOF. Instead of prescribing fixed splines, ranges of permissible motion were identified for each flexion-extension DOF which better captured participant-specific variability.

Similarly, Marieswaran et al. (2018) implemented a six-DOF knee model in *OpenSim*, with MRI-informed cartilage and menisci for ligament elastic properties and geometry. These findings reinforce that unlocking or modifying joint constraints enables more biofidelic predictions of joint loading and ligament strain for varying populations or tasks. However, a key challenge in implementing multi-DOF joint definitions is that many of these additional degrees of freedom are difficult to capture accurately using marker-based motion capture, which can introduce noise and error into the kinematic estimates due to soft tissue artifact (Cereatti et al., 2017). As such, more complex joint representations are not always feasible or appropriate depending on the available data and desired application.

Despite these advances across all personalization levels (bones, muscles, ligaments, and joint definitions), most studies implement multiple modifications simultaneously which makes it difficult to isolate the specific contribution of bone geometry to simulation outcomes. In pediatric modelling, it would be valuable to understand how each of these personalization levels can impact simulation outcomes, and the sensitivity to the levels independently. Addressing this gap would allow for essential understanding of the independent value of anatomical fidelity in skeletal structures.

1.4.3 Model Personalization Pipelines

Various open-source pipelines have emerged to incorporate participant-specific anatomy into MSK models, with the aim of increasing biomechanical fidelity while reducing the manual workload of implementation. Among the options is *MAP Client* which facilitates participant-specific model creation using MRI data, motion capture, and statistical shape models (Zhang et al., 2016). Its workflow is capable of aligning geometries through non-rigid registration to landmarks, and iterative principal component fitting. The main strength of the *MAP Client* lies in its flexibility, but this comes at the cost of operator time and expertise.

The *Insigneo* pipeline offers a highly detailed, MRI-driven approach to creating full lower-limb MSK models (Modenese et al., 2018). Segmented MRI bones are aligned using statistical shape models, and muscle attachments are transferred via affine transformations from an atlas based on anatomical landmarks. *Insigneo* is one of the most comprehensive pipelines for muscle-inclusive participant-specific modelling, yet the complexity of the steps results in a processing time of roughly 10 hours per limb which limits its feasibility for large cohorts.

The *STAPLE* pipeline addresses this time burden by fully automating skeletal model formation from pre-segmented bone geometries (Modenese et al., 2021). A key feature of *STAPLE* is its ability to define joint coordinate systems (JCS) from bone shapes using geometric algorithms such as geometry-informed biomechanical optimization and classification (GIBOC), Kai, and central shift methods. Each approach offers varying degrees of anatomical fidelity, reproducibility, and processing complexity. The GIBOC method defines anatomical coordinate systems based on the curvature of articular surfaces, such as the femoral condyles, enabling reconstruction of clinically meaningful axes (Renault et al., 2018). The Kai method establishes coordinate systems by fitting geometric shapes, such as spheres and ellipses, to bone surfaces and landmarks prioritizing reproducibility across femur, pelvis, and tibia bone geometries (Kai et al., 2014). The centroid shift method can leverage existing *STAPLE* utilities to compute transformations between generic and participant-specific bones by aligning their geometric centroids which offers a fast and reproducible alternative that integrates seamlessly with STAPLE's automated framework. In this study, the centroid shift was purposefully selected to maintain a consistent, scalable pipeline that could accommodate and rapidly generate participant-specific skeletal models across a full dataset. While methods like GIBOC and Kai offer richer anatomical detail, centroid shift aligns more

closely with the practical aims of this work to minimize manual intervention, maximize throughput and ensure standardized joint definitions across participants. This makes the centroid shift method well-suited for studies focused on group-level comparisons where consistency and scalability may outweigh marginal anatomical gains in joint axis definition.

Overall, *STAPLE* can balance automation, reproducibility, and compatibility with *OpenSim* which enables efficient integration of segmented bones into personalized skeletal models. The modularity found in *STAPLE* allows for future expansion into automated MSK modelling, and is one of the current, fastest ways to generate these articulated *OpenSim*-compatible skeletal models.

Finally, *nmsBuilder* is a freeware to create participant-specific MSK models for *OpenSim*. It functions more as a toolkit than a pipeline, offering a manual general user interface for defining joint coordinate systems, and refining inertial parameters (Valente et al., 2017). It is often used in tandem with pipelines like *Insigneo* or *STAPLE* for visualization, validation, or fine-tuning of joint coordinate placement; however, its primary advantage is anatomical precision based on manual adjustment which means extensive manual input – its main drawback (Princelle et al., 2023). Overall, the choice of pipeline, and the degree of its use, depends on the project's needs, such as *Insigneo* for full-body musculature or *STAPLE* for rapid skeletal model generation.

Among these options, *STAPLE* offers a favourable balance between automation, reproducibility, and *OpenSim* compatibility which makes it well-suited for studies containing larger groups. One notable requirement of the *STAPLE* pipeline is the use of full bone geometries to enable accurate joint coordinate definitions. Thus, when full participant-specific segmentation is not available, researchers must address this by first registering generic model bone geometries to the available partial geometry of the participant for the skeletal model generation.

1.4.4 Medical Imaging and Segmentation

Musculoskeletal (MSK) models rely on accurate anatomical representations of bones and joints, which are often derived from medical imaging. Magnetic resonance imaging (MRI) is used to capture high-resolution images of both soft tissue and bone and is often employed in the assessment of knee joint injuries, including anterior cruciate ligament ruptures (Kocabey et al., 2004). While conventional use of MRI involves 2D slice-based interpretation, converting these slices into three-dimensional reconstructions improves both the accuracy and clarity of anatomical features when compared to 2D methods (Sartoretti et al., 2022). The creation of 3D models from MRI data requires a segmentation process where the structures of interest are identified across image slices and reconstructed into complete volumetric structures.

Several software platforms are available for segmentation, and one commonly used tool is the Medical Imaging Interaction Toolkit (*MITK*) which enables precise manual segmentation through a 2D slice-by-slice interface (Figure 1.2A). While anatomically detailed, this method is often time-consuming, requires significant user training, and lacks real-time 3D feedback. In contrast, newer platforms, such as *Elucis* (RealizeMedical, 2021) have adopted immersive 3D environments, leveraging either virtual reality or screen-based interaction, to simplify segmentation (Figure 1.2B). This platform offers real-time structure volume manipulation and claims reduced learning times which leads to faster and more intuitive segmentation, particularly for users with limited experience in medical imaging.

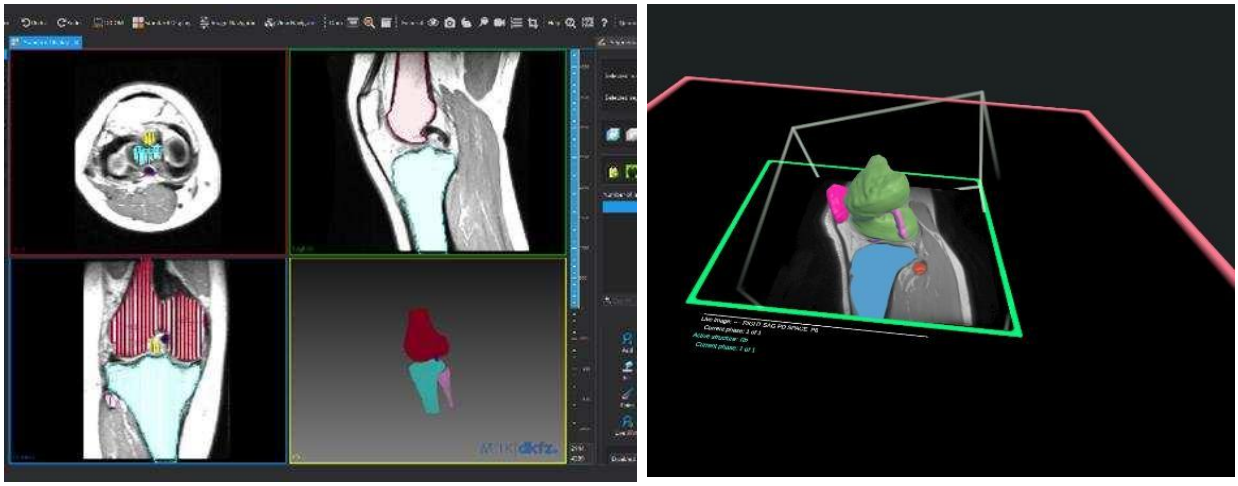

A. *MITK* – Single Frame of post- segmentation view B. *Elucis* – 3D Immersion of post-segmentation view

Figure 1.2: Segmentation software platforms, MITK (A) and Elucis (B), during smoothing and accuracy verification post-participant geometry segmentation of the structures of interest

However, as novel 3D segmentation tools become more accessible, their potential to reduce segmentation time and improve usability must be balanced against the need to maintain anatomical accuracy. Understanding how different software platforms perform in terms of efficiency and reliability is important when selecting appropriate tools for modelling applications that rely on participant-specific anatomy and will be addressed in Study 1 of this thesis.

1.4.5 Geometry Registration

Participant-specific MSK modelling often begins with segmenting bones from medical imaging data. However, these segmented geometries cannot be used directly in a simulation framework, they must first be aligned with the existing model structure. This process, known as geometry registration, ensures that the segmented bones are oriented, scaled, and positioned consistently with the generic model. In many cases, particularly in pediatric imaging or limited field-of-view scans, only a partial bone may be available. In such scenarios, additional steps are required to reconstruct the missing portions of the bone before it can be substituted into the model. Together, alignment and reconstruction form the core of geometry registration workflows with a generic model.

Several registration strategies are available depending on the completeness of the segmented bone, and the level of anatomical fidelity required. There is rigid registration which provides coarse alignment through rotational and translational transformation. Also, there is non-rigid registration which allows localized deformations for closer surface matching. Then, there are statistical shape models (SSMs) which enable estimation of missing bone geometry based on population-level anatomical variation. These strategies all enable downstream substitution or deformation of the generic model's geometry while maintaining kinematic and anatomical consistency.

A workflow-based approach that can be used for geometry personalization is the Musculoskeletal Atlas Project (*MAP*) Client, which along with the capability of building the final MSK model can first register the participant-specific bone to the generic bone prior to model geometry substitution and replacing geometry dependencies (*MAP Client* Documentation, 2024). A key feature of *MAP* is its integration with SSMs, which use population-level variation to deform generic geometries toward participant-specific anatomy based on sparse landmarks or segmented

surfaces. This principal component analysis (PCA)-driven deformation enables non-rigid alignment of bones, though *MAP* workflows typically require substantial manual setup and domain knowledge, limiting their scalability for larger datasets (Zhang et al., 2016).

SSMs can also be applied outside of *MAP* pipelines, offering an alternative approach for geometry reconstruction when segmentations are available. By training on aligned population data, SSMs can predict full bone shapes from a small number of surface landmarks, an approach that has been used in pediatric orthopaedics to reconstruct lower-limb bone geometries (Nolte et al., 2016; Warren et al., 2022). However, their reliance on training data limits their accuracy in populations with atypical or pathological morphology.

Next, when full bone or partial geometry is available, rigid registration is often used to align the segmented bones. In full bone cases, this can be where the process ends, but for partial geometries, more steps may be required. Rigid registration, using the numerical method of iterative closest point (ICP), works to minimize the Euclidean distance between two sets of surface points by iteratively estimating the optimal rotation and translation that aligns them (Besl et al., 1992). As rigid ICP only allows for six degrees of freedom (DOF; three translational, three rotational), rigid ICP cannot account for anatomical differences in shape, rather it is best suited for coarse, global alignment.

For further morphological alignment in full bone or participant-specific geometries, non-rigid registration can be used. Free-form non-rigid registration methods, like Coherent Point Drift (CPD), operate on segmented geometries and allow mesh deformation without being bound to population averages unlike SSM approaches. Non-rigid ICP incorporates local affine transformations or spline-based warping to flexibly adapt one geometry mesh to another (Amberg et al., 2007, Brown et al., 2004). However, non-rigid ICP can introduce unrealistic distortions when applied to complex biological shapes, especially without sufficient regularization (Kundu et al., 2024).

To address these challenges, Coherent Point Drift (CPD) offers more robust deformation control. CPD aligns two shapes by treating one mesh as a probabilistic distribution and allowing smooth deformation towards the target mesh (Myronenko et al., 2010). CPD is well-suited to biological geometries, like bones, where natural variation in shape occurs gradually rather than abruptly. CPD avoids unrealistic warping which allows for local deformations to improve the surface matching.

In summary, geometry registrations can be approached through rigid registration (e.g., ICP), non-rigid methods (e.g., CPD), or statistical shape modelling (e.g., PCA-based SSMs), each with its own advantages depending on the completeness of the geometry and the required fidelity. Rigid ICP offers efficient global alignment, while SSMs enable population-based reconstruction from sparse data, and CPD allows flexible, localized deformation without relying on populations. In Study 2, rigid ICP was used for coarse alignment, followed by CPD for non-rigid surface conformation. This hybrid approach allowed for a balance between anatomical specificity and computational efficiency which enabled personalization of femur and tibia geometries in the absence of full bone geometries.

1.5 Task Selection

The forward lunge is a widely used movement in both clinical rehabilitation and biomechanical research, as it's a closed kinetic chain task and minimizes the sudden force input through the joint (Alkjaer et al., 2012). For biomechanical assessment, forward lunges allow for good test-retest

reliability and producing consistent levels of tissue stress (Alkjaer et al., 2020, Comfort et al., 2015). Compared to more dynamic tasks like cutting or pivoting, the lunge provides a safer, more controlled loading environment for the knee joint. As this movement is functional and replicable, it is well-suited for evaluating joint mechanics in both experimental and simulated conditions and will be used in Study 2 to assess whether incorporating personalized knee bone geometries into an *OpenSim* model affects joint center location, knee kinematics, and marker tracking error compared to a fully generic model.

1.6 Study Motivation and Research Gaps

This thesis addresses two distinct but interconnected research questions that arise across the imaging-to-simulation pipeline in MSK modelling. Each study targets a different stage, segmentation (Study 1) and simulation (Study 2), with the overall goal of identifying practical and methodological considerations in developing participant-specific knee models.

1.6.1 Study 1: Segmentation Agreement

One of the initial stages in developing personalized models is the segmentation of anatomical structures from medical images. While a variety of segmentation platforms exist, they vary in interface design, user workflow, time efficiency, and anatomical control. Traditional platforms, such as *MITK*, offer detailed, slice-by-slice control but are time-consuming and require user expertise. In contrast, emerging tools like *Elucis* aim to streamline segmentation using immersive 3D environments, reducing the learning curve and enabling faster manipulation of structures. However, the trade-off between speed and segmentation accuracy remains unclear.

Gap: There is limited research comparing segmentation platforms in terms of both time-efficiency and anatomical agreement for traditional segmentation against virtual-reality-based segmentation.

Aim: To quantitatively compare segmentation time (using femur, tibia, fibula, PCL, and ACL) and surface geometry agreement (using femur, tibia, fibula, and PCL) between *MITK* and *Elucis* software platforms using 3D reconstruction.

Hypothesis: Using *Elucis* software will reduce segmentation time without compromising the geometric agreement of the resulting bone models relative to using *MITK* software.

1.6.2 Study 2: Modelling with Partial Participant-Specific Geometry

While participant-specific modelling is known to improve anatomical realism, most studies incorporate multiple personalization features simultaneously (e.g., bone, muscles, ligaments, and joint definitions), making it difficult to isolate the specific impact of any one factor. In pediatric modelling, where growth-related anatomical variability is high, it remains unclear whether the integration of personalized bone geometry alone is sufficient to influence simulation outputs.

Gap: There is a lack of knowledge about the independent effect of participant-specific bone geometry on MSK kinematic simulation outcomes, particularly in pediatric populations.

Aim: To assess whether incorporating personalized femur and tibia geometries into a generic *OpenSim* model affects joint center location, knee kinematics, and marker tracking error compared to a fully generic model.

Hypothesis: Participant-specific models will yield measurable differences in knee joint center, knee flexion angle, and reduce marker error even in the absence of other personalized features.

Together, these studies provide a focused examination of both early and late stages of a MSK modelling pipeline. Study 1 explores how segmentation tools may affect efficiency and accuracy in generating anatomical geometries, while Study 2 examines how these personalized geometries, once incorporated into musculoskeletal models, influence biomechanical simulation outcomes. In doing so, this thesis provides insight into the practical trade-off between efficiency, accuracy, and bio-fidelity when creating participant-specific knee models.

Chapter 2: MANUSCRIPT 1

3D Modelling from MRI of pediatric knees using virtual reality and segmentation platforms: An inter-rater and inter-software comparison

Elese St Louis [1], Blake Miller [1, 2], Allison Clouthier [3], Daniel L. Benoit[4], Sasha Carsen[5], and Teresa Flaxman [2]

[1] Faculty of Engineering, University of Ottawa, Canada
[2] Clinical Epidemiology Program, Ottawa Hospital Research Institute
[3] School of Human Kinetics, University of Ottawa, Canada
[4] Faculty of Medicine, Lund University, Sweden
[5] Division of Orthopaedics, Children's Hospital of Eastern Ontario, Canada

Abstract

Magnetic resonance imaging (MRI) is essential for evaluating knee injuries, particularly anterior cruciate ligament (ACL) injuries in pediatric populations. Traditional 2D segmentation software, such as *MITK* (Medical Imaging Interaction Toolkit), is widely used but requires more in-depth knowledge of medical imaging principles (e.g., recognizing modality-specific artifacts) and can be time intensive. Virtual reality-based segmentation, such as *Elucis* (Realize Medical), may improve segmentation efficiency while maintaining accuracy. This study compares inter-rater reliability, inter-software agreement, and segmentation efficiency between *MITK* and *Elucis* done by two raters. Dice Similarity Coefficient (DSC, 1 = perfect match) scores assessed segmentation agreement for the femur, tibia, fibula, and posterior cruciate ligament (PCL). *Elucis* demonstrated similar inter-software agreement for the femur, tibia and fibula (DSC $\geq$ 0.90) and improved reliability for the PCL (DSC = 0.77 vs. 0.57). Segmentation time was significantly reduced with *Elucis*, averaging 8.6 minutes less per segmentation ($p < 0.001$). These findings suggest that *Elucis* is a viable alternative for pediatric knee segmentation as it offers good agreement with MITK with improved efficiency.

2.1 Introduction

Magnetic resonance imaging (MRI) is widely used to assess knee injuries and pathology in both adult and pediatric populations (Kocabey et al., 2004). MRIs provide clinicians with high-resolution images to evaluate joint anatomy to diagnose conditions, plan surgical interventions, and/or monitor post-treatment recovery. A crucial step in leveraging MRI data is segmentation, where anatomical structures are isolated in each 2D slice to create 3D models. These models have the potential to enhance clinical decision making by offering detailed anatomical visualization, improving surgical planning, and facilitating patient education (Brady et al., 2022; Morris et al., 2021). In pediatric care, interactive 3D models could help young patients to better understand their injuries which could foster engagement in their treatment plan. However, generating these models is time-intensive and typically performed by specialized technicians, radiologists, or researchers. The increasing demand for participant-specific models highlights the urgent need for advanced segmentation tools that streamline the process for creating 3D models. By improving segmentation efficiency, more 3D models can be created, allowing a greater number of patients to visualize their own anatomy, comprehend their condition, and feel more informed about surgical interventions (Martel-Pelletier et al., 2023).

Segmentation methods vary from manual to automatic techniques with standard 2D software, such as the Medical Imaging Interaction Toolkit (*MITK*, Germany), being widely used for manual segmentation. While reliable, 2D software is time intensive, requires specialized training, and uses substantial user input (Nayak et al., 2021; Rogelj et al., 2022; Chandra et al., 2018). Automatic segmentation techniques have been developed, particularly for bone imaging via computed tomography (CT), which has been shown to have high accuracy and efficiency (Lenchik et al., 2019). However, automatic segmentation for soft tissue structures via MRI, such as menisci and ligaments, remain unreliable due to high variability and overestimation of tissue volumes (Harkey et al., 2022; Paproki et al., 2017; Tang et al., 2022; Trimpl et al., 2022). Therefore, manual and semi-automatic segmentation approaches remain the preferred options for MRI-based knee modelling.

Emerging 3D virtual reality (VR) segmentation software, such as *Elucis* (RealizeMedical, Ottawa, Canada), offers an alternative that may improve efficiency and user experience. Unlike traditional 2D platforms, VR-based tools allow users to interact with medical images in a three-dimensional environment, offering more intuitive spatial manipulation and visualization (Preukschas et al., 2024; Johnston et al., 2018; Nolden et al., 2013). Prior research suggests that VR segmentation enhances user engagement, reduces cognitive load, and improves spatial accuracy (Martel-Pelletier et al., 2023; Liimatainen et al., 2021). However, the effectiveness for knee MRI segmentation has not yet been validated, and some researchers remain skeptical of VR-based segmentation due to its cost, accessibility, and potential variability in user experience (Hornsey et al., 2024).

This study aims to compare the segmentation agreement, inter-rater reliability, and time efficiency of *Elucis* and *MITK* for segmenting pediatric knee MRI data. It is hypothesized that *Elucis* will yield similar volumes to *MITK* while significantly reducing segmentation time. By evaluating the feasibility of VR-based segmentation, this study contributes to the development of efficient and accurate 3D modelling approaches for orthopedic and biomechanical applications.

2.2 Materials and Methods

This study followed a retrospective observational design and adhered to the Guideline for Reporting Reliability and Agreement Studies (GRRAS) recommendations for reliability studies (Kottner er al., 2011). Ethical approval was obtained from the Children's Hospital of Eastern Ontario, the University of Ottawa, and the Ottawa Hospital. A cohort of pediatric participants who underwent pre-operative knee MRI scans for an expected anterior cruciate ligament (ACL) rupture was selected.

Inclusion criteria were female athletes with a confirmed ACL rupture who received an MRI as standard care, aged 8 -18 years old, who participated in organized sports prior to injury. Exclusion criteria consisted of any participants who encountered a lower limb injury (other than ACL rupture) within the past six months to minimize confounding effects on knee anatomy. A total of 33 female participants (age: 15.4 ± 1.3 yrs; height: 165.4 ± 5.7 cm; mass 64.7 ± 10.6 kg; mean ± standard deviation) were randomly selected. One rater segmented all 33 participants using both software platforms, while a randomly selected subset of 16 participants were also analyzed by a second rater to assess for inter-rater reliability.

MRI data were acquired using either GE 1.5T (n=24) or Siemens 3T (n=9) scanners. Only sagittal proton density cube sequences (SAG PD Cube) were used for segmentation. Imaging parameters included a slice thickness of 3.0 - 3.5 mm, an interslice gap of 0.3 - 1.0 mm, and field of view extending approximately ± 150 mm from the tibiofemoral joint space (Figure 2.1). All scans were acquired with anisotropic voxels, and the acquisition plane was oriented near-true sagittal (< 6°) to the femoral condyles. Protocol-specific settings for each scanner (repetition/echo times, flip angle, in-plane resolution, and bandwidth) are summarized in Table B.1.

Figure 2.1: DICOM file of sagittal knee MRI scan from single participant via MicroDicom DICOM viewer (2024.1, Bulgaria) showing the available structures for segmentation from the tibiofemoral joint

Segmentation was performed using *MITK* (Medical Imaging Interaction Toolkit, Workbench 2018.04.2, Germany) for 2D segmentation, and *Elucis* (RealizeMedical, Canada) for 3D virtual reality segmentation. Two raters independently segmented the MRI scans following software-specific workflows, and after receiving a one-day workshop training on *MITK* (Figure A.1). In *MITK*, images were manually segmented using 2D tools such as "add" and "subtract", with masks created every 3 - 4 slices in areas of low surface variability, or more frequently in areas of high surface variability. 3D interpolation was applied to complete 3D geometries which were further refined using MeshLab (2023.12, Italy) for post-processing. Due to software limitations, thresholding was not used in *MITK*. In *Elucis*, segmentations involved an initial "addition" tool,

followed by intensity-based thresholding (2600 - 6600 pixels) using the "grow" function. Manual refinements with the "subtraction" and "shrink" tools were applied, and final smoothing operations were performed in *Elucis* to refine the 3D structure.

To assess segmentation accuracy, the Dice Similarity Coefficient (DSC) was calculated, quantifying spatial overlap between *MITK* and *Elucis* segmentations (Zou et al., 2004). The DSC formula is given as

$$DSC = \frac{2\,|X \cap Y|}{|X|+|Y|}, \quad (1)$$

where X and Y represent binary spatial mappings of segmented structures. DSC scores were computed using 3D Slicer (v5.6.1, USA) via the "Segment Comparison" plugin (Figure 2.2). Two comparisons were made: (1) inter-rater agreement, comparing segmentations from two raters within each software, and (2) inter-software agreement, comparing the same rater's segmentations between *MITK* and *Elucis*. DSC values were evaluated for four structures: the femur and tibia (large structures; threshold DSC ≥ 0.85) and the fibula and posterior cruciate ligament (PCL; small structures; threshold DSC ≥ 0.65). As no clearly defined threshold for an 'acceptable' DSC exists in literature, a threshold for acceptable agreement for large and small structures was selected based on the mid-point of existing literature (Palumbo et al., 2019; Juras et al., 2020; Korte et al., 2021; Kway et al., 2021; Deeley et al., 2011). The ACL was ruptured, so it was not included in the DSC reporting.

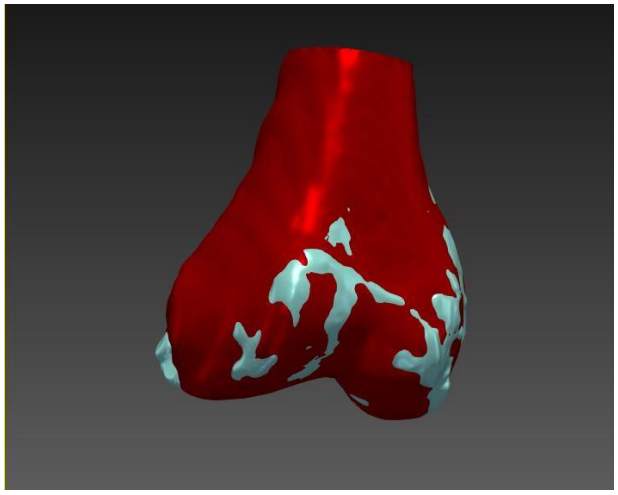

Figure 2.2: Segmented participant-specific femur geometries from Elucis (red) and MITK (blue) overlayed on MITK to showcase intersecting geometries

Segmentation time was recorded for each participant across five knee structures: femur, tibia, fibula, ACL, and PCL. For inter-software comparisons, times were recorded for a single rater using both *MITK* and *Elucis*. For inter-rater comparisons, segmentation times were recorded separately for both raters within each software.

Paired t-tests were used to assess differences in segmentation time. If normality assumptions were not met, Wilcoxon signed-rank tests were applied as a non-parametric alternative. Sample size calculations for time analysis was conducted using G*Power (v3.1.9.2, Germany), yielding a required sample size of 14 participants (effect size = 0.821; α = 0.05; power = 0.80). However, to enhance the reliability and generalizability of the findings, a larger sample was used. Thus, inter-software comparisons included all 33 participants, while inter-rater reliability analysis was performed on a subset of 16 participants.

2.3 Results

This study evaluated segmentation agreement, reliability, and efficiency between *MITK* and *Elucis* for pediatric knee MRI analysis.

2.3.1 Segmentation Agreement and Reliability

2.3.1.1 Inter-software Agreement (MITK vs. Elucis Comparisons)

Inter-software agreement was assessed for both large (femur, tibia) and small (fibula, PCL) structures using DSC obtained from a single rater segmenting in both platforms (Table 2.1). The femur demonstrated strong inter-software agreement with an average DSC of 0.90, exceeding the predefined threshold (≥ 0.85). The tibia showed similar high agreement (DSC – 0.93). The fibula demonstrated strong agreement (DSC – 0.90) still exceeding the threshold (≥ 0.65), but with greater variability. PCL had the lowest agreement, falling below the acceptable threshold (≥ 0.65).

Table 2.1: Inter-software (MITK vs. Elucis) and inter-rater (Rater 1 vs. Rater 2) agreement based on Dice Similarity Coefficient (DSC) for the femur, tibia, fibula, and PCL.

	Rater	Software	Structure	**DSC** Mean [Range]
Inter-software	Rater 1 (n = 33)	*MITK* v. *Elucis*	Femur	0.90 [0.74 - 0.96]
			Tibia	0.93 [0.75 - 0.98]
			Fibula	0.90 [0.67 - 0.95]
			PCL	0.64 [0.16 - 0.82]
Inter-rater	Rater 1 v. Rater 2 (n = 16)	*MITK*	Femur	0.96 [0.92 - 0.97]
			Tibia	0.96 [0.95 - 0.97]
			Fibula	0.91 [0.87 - 0.97]
			PCL	0.57 [0.46 - 0.67]
		Elucis	Femur	0.96 [0.85 - 0.98]
			Tibia	0.96 [0.93 - 0.98]
			Fibula	0.93 [0.87 - 0.97]
			PCL	0.77 [0.58 - 0.87]

2.3.1.2 Inter-rater Reliability (Rater 1 vs. Rater 2)

Inter-rater reliability was assessed by comparing segmentations from two independent raters (n = 2) within each software (Table 2.1). High inter-rater DSC values were observed for both femur and tibia (DSC – 0.96; MITK and Elucis), exceeding the threshold (≥ 0.85). The fibula also demonstrated acceptable reliability, though with slightly lower DSC values (DSC – 0.91 in MITK; 0.93 in Elucis). PCL showed weaker reproducibility, with MITK (DSC - 0.57) falling below threshold and Elucis (DSC - 0.77) exceeding it.

2.3.2 Segmentation Efficiency

Segmentation efficiency was evaluated based on the total time taken to segment five knee structures (femur, tibia, fibula, PCL, and ACL). Time comparisons were made for inter-software (*MITK* v. *Elucis*) and inter-rater (Rater 1 v. Rater 2) segmentations. For inter-rater efficiency, the time difference between Rater 1 and Rater 2 was 17.79 minutes in *MITK* and 19.76 minutes in *Elucis*, both of which were significant ($p < 0.001$) (Table 2.2). For inter-software efficiency, *Elucis*, on average, required 8.6 minutes less than *MITK* for segmentations ($p < 0.001$). These results suggest that *Elucis* is significantly faster than *MITK*, reducing segmentation time without compromising segmentation quality.

Table 2.2: Segmentation times for inter-rater (Rater 1 v. Rater 2) comparisons across knee structures. Absolute time differences between raters are shown with significance, assessed using paired t-tests.

Analysis	Software	Variable	Rater 1 (min)	Rater 2 (min)	|Rater 1 - Rater 2| (min)	Between rater p-value
Inter-Rater (Rater 1 v. Rater 2 (*n=16*))	***MITK***	Mean	40.03	20.92	17.79	
		Std Deviation	9.91	4.49	11.65	<0.001
		Range	14.28 - 58.76	11.90 - 32.16	11.58 - 24.00	
	Elucis	Mean	30.76	13.54	19.76	
		Std Deviation	10.26	2.80	13.65	<0.001
		Range	19.87 - 41.85	9.70 - 21.02	12.20 - 27.32	

2.4 Discussion/Conclusion

The purpose of this study was to evaluate whether *Elucis*, a VR-based segmentation tool, could achieve comparable segmentation agreement, reliability, and time efficiency relative to MITK, a 2D segmentation software.

Across large bony structures, both software performed consistently. All femur DSC values exceeded the 0.85 agreement threshold for both MITK and Elucis, and tibia segmentations similarly showed high inter-software agreement (average DSC – 0.93). For the fibula, inter-software DSC values varied more with some low values, but the average was still above threshold. The PCL demonstrated the weakest agreement (DSC – 0.64) and fell below the predefined benchmark. These findings suggest that large bone structures such as femur and tibia are robustly segmented with both tools, whereas, smaller or soft tissue structures, like the fibula and PCL, remain more sensitive to software differences. This is consistent with previous reports that smaller anatomical features are more challenging to segment reliably, as their size and imaging characteristics increase variability (Johnston et al., 2018; Liimatainen et al., 2021).

Inter-rater reliability analyses demonstrated strong agreement for the femur and tibia in both MITK and Elucis (average DSC – 0.96) with slightly lower values for the fibula (0.91 – 0.93) and the PCL (0.57 in MITK; 0.77 in Elucis). These results again highlight that large structures are consistently reproducible across raters, while smaller, soft tissue structures present greater challenges. Importantly, although Elucis showed high inter-rater DSC than MITK for the PCL, the

variability remained evident, showing that segmentation of small, soft tissue structures is difficult regardless of software (Kway et al, 2021; Deeley et al., 2011; Fiederer et al., 2019). These findings align with previous work reporting that VR-based segmentation tools can reduce, but not eliminate, user variability by enabling more intuitive interaction with complex anatomy (Fiederer et al., 2019; Duncan et al., 2019). Also, given that the PCL was able to exceed the reliability threshold suggests the advantages of VR-based segmentation in providing reliable segmentations, consistent with prior studies emphasizing the precision and enhanced visual capabilities of VR over traditional 2D methods (Johnston et al., 2018; Satava et al., 1998; Liimatainen et al., 2021). Standardizing evaluation metrics, such as tailoring DSC thresholds to structure size and tissue characteristics, may further improve the comparability of segmentation studies across different tools and anatomical targets (Palumbo et al., 2019; Juras et al., 2020; Korte et al., 2021; Kway et al., 2021; Deeley et al., 2011; Fiederer et al., 2019; Duncan et al., 2019; Maier-Hein et al., 2018).

Segmentation efficiency also differed between software. Elucis demonstrated an average time savings of 8.6 minutes per segmentation compared to MITK, representing a 21% reduction. Both raters achieved faster segmentation times with Elucis, regardless of individual style. While this suggests that immersive VR interfaces may streamline the segmentation workflow, efficiency must be considered along with agreement and reliability outcomes, as the clinical and research relevance of time savings depend on study context and structural complexity (Scheys et al., 2011; Carriero et al., 2009). Segmentation efficiency is an important consideration as the ability to rapidly produce participant-specific 3D models can enhance patient care through providing surgeons with precise anatomical details, more frequent and detailed disease monitoring assessments, and expanding the feasibility of participant-specific modelling in research and clinical practice (Scheys et al., 2011; Carriero et al., 2009; Smale et al., 2019).

Limitations of this study included anatomical exactness, assessor experience, rater sample size, and imaging protocols. Anatomical exactness of the segmented geometries was not addressed, rather the focus was on comparing the degree of agreement between MITK and Elucis. As such, the study does not establish which software produced the "most correct" segmentation relative to a gold standard. Another limitation was assessor experience as both raters had less than one year of working with either software at the time of the study, and no expert raters were included. While this level of experience may reflect typical research uses, it limits the generalizability of the findings to more clinical experienced populations. In addition, only two raters (N = 2) were included, which constrains the reliability assessment and prevents broader conclusions about inter-rater variability. Finally differences in imaging protocols between participants (e.g., variations in magnetic field strength or in plane resolution) may have contributed to segmentation variability and influenced results.

Further studies should address these limitations by incorporating expert raters, expanding the number of assessors, and validating segmentation results against anatomical ground truths. In addition, further work is needed to examine segmentation performance across different anatomical regions and imaging modalities, as well as to evaluate clinical applications of VR- and 2D-based tools. Consideration of training requirements and cost-effectiveness will also be important for understanding how such tools can be implemented in practice.

Conflict of Interest:
One co-author (T. Flaxman) has collaborated with an individual who is currently on the advisory board of the company that develops Elucis. This relationship did not influence the design, conduct, or reporting of this study. Realize Medical provided access to the software; however, they did not review or provide any feedback on study design, data analysis and interpretation, or the manuscript.

2.5 References

Brady, A., Beets-Tan, R., Brkljačić, B., et al. (2022). The role of radiologist in the changing world of healthcare: a white paper of the european society of radiology (ESR). *Insights into Imaging*, *13*(100), 1-6. https://doi.org/10.1186/s13244-021-01156-7.

Carriero, A., Zavatsky, A., Stebbins, J., Theologis, T., Shefelbine, S. (2009). Correlation between lower limb bone morphology and gait characteristics in children with spastic diplegic cerebral palsy. *Journal of Pediatric Orthopaedics*, *29*, 73-79. https://doi.org/10.1097/BPO.0b013e318193450a.

Chandra, S., Dowling, J., Engstrom, C., Xia, Y., Paproki, A., Neubert, A., Rivest-Henault, D., Salvado, O., Crozier, S., Fripp, J. (2018). A lightweight rapid application development framework for biomedical image analysis. *Computer Methods and Programs Biomedicine, 164,* 193-205. https://doi.org/10.1016/j.cmpb.2018.06.017.

Deeley, M., Chen, A., Datteri, R., Noble, J., Cmelak, A., Donnelly, E., Malcolm, A., Moretti, L., Jaboin, J., Niermann, K., Yang, E., Yu, D., Yei, F., Koyama, T., Ding, G., Dawant, B. (2011). Comparison of manual and automatic segmentation methods for brain structures in the presence of space-occupying lesions: a multi-expert study. *Physics in Medicine and Biology, 56(*14), 4557–4577. https://doi.org/10.1088/0031-9155/56/14/017.

Duncan, D., Garner, R., Zrantchev, I., Ard, T., Newman, B., Saslow, A., Wanserski, E., Toga, A. (2019). Using virtual reality to improve performance and user experience in manual correction of MRI segmentation errors by non-experts. *Journal of Digital Imaging, 32,* 97-104. https://doi.org/10.1007/s10278-018-0120-1.

Fiederer, L., Alwanni, H., Völker, M., Schnell, O., Beck, J., Ball, T. (2019). A research framework for virtual reality neurosurgery based on open-source tools. *IEEE Transactions on Biomedical Engineering, 66,* 2120-2132. https://doi.org/10.1109/TBME.2019.2901523.

Harkey, M., Michel, N., Kuenze, C., Fajardo, R., Salzler, M., Driban, J., Hacihaliloglu, I. (2022). Validating a semi-automated technique for segmenting femoral articular cartilage on ultrasound images. *Cartilage, 13*(2), 194760352210861. https://doi.org/10.1177/19476035221086112.

Hornsey, R., Hibbard, P. (2024). Current perceptions of virtual reality technology. *Applied Sciences, 14*(10), 4222. https://doi.org/10.3390/app14104222.

Johnston, A., Rae, J., Ariotti, N., Bailey, B., Lilja, A., Webb, R., Ferguson, C., Maher, S., Davis, T., Webb, R., McGhee, J., Parton, R. (2018). Journey to the centre of the cell: Virtual reality immersion into scientific data. *Traffic, 19*(2), 105-110. https://doi.org/10.1111/tra.12538.

Juras, V., Szomolanyi, P., Schreiner, M., Unterberger, K., Kurekova, A., Hager, B., Laurent, D., Raithel, E., Meyer, H., Trattnig, S. (2020). Reproducibility of an automated quantitative MRI assessment of low-grade knee articular cartilage lesions. *Journal of Imaging, 6,* 125. https://doi.org/10.3390/jimaging6110125.

Kocabey, Y., Tetik, O., Isbell, W., Atay, O., Johnson, D. (2004). The value of clinical examination versus magnetic resonance imaging in the diagnosis of meniscal tears and anterior cruciate ligament rupture. *Arthroscopy, 20*, 696-700. https://doi.org/10.1016/j.arthro.2004.07.007.

Korte, J., Hardcastle, N., Ng, S., Clark, B., Kron, T., Jackson, P. (2021). Cascaded deep learning-based auto-segmentation for head and neck cancer patients: Organs at risk on T2-weighted magnetic resonance imaging. *Medical Physics, 48*, 1348–1359. https://doi.org/10.1002/mp.14680.

Kottner, J., Audigé, L., Brorson, S., Donner, A., Gajewski, B., Hróbjartsson, A., Roberts, C., Shoukri, M., Streiner, D. (2011). Guidelines for reporting reliability and agreement studies (GRRAS) were proposed. *Journal of Clinical Epidemiology, 64*(1), 96–106. https://doi.org/10.1016/j.jclinepi.2010.03.002.

Kway, Y., Thirumurugan, K., Tint, M., Michael, N., Shek, L., Yap, F., Tan, K., Godfrey, K., Chong, Y., Fortier, M., Marx, U., Eriksson, J., Lee, Y., Velan, S., Feng, M., Sadananthan, S. (2021). Automated segmentation of visceral, deep subcutaneous, and superficial subcutaneous adipose tissue volumes in MRI of neonates and young Children. *Radiology: Artificial Intelligence, 3*(5), e200140.https://doi.org/10.1148/ryai.2021200140.

Lenchik, L., Heacock, L., Weaver, A., Boutin, R., Cook, T., Itri, J., Filippi, C., Gullapalli, R., Lee, J., Zagurovskaya, M., Retson, T., Godwin, K., Nicholson, J., Narayana, P. (2019). Automated segmentation of tissues using CT and MRI: A systematic review. *Academic Radiology, 26*(12), 1695-1706. https://doi.org/10.1016/j.acra.2019.08.006.

Liimatainen, K., Latonen, L., Valkonen, M., Kartasalo, K., Ruusuvuori, P. (2021). Virtual Reality for 3D histology: multi-scale visualization of organs with interactive feature exploration. *BMC Cancer, 21*(1), 1220. https://doi.org/10.1186/s12885-021-08964-0.

Maier-Hein, L., Eisenmann, M., Reinke, A., Onogur, S., Stankovic, M., Scholz, P., Stock, C. (2018). Why rankings of biomedical image analysis competitions should be interpreted with care. *Nature Communications, 9*, 5217. https://doi.org/10.1038/s41467-018-07619-7.

Martel-Pelletier, J., Paiement, P., Pelletier, J.-P. (2023). Magnetic resonance imaging assessments for knee segmentation and their use in combination with machine/deep learning as predictors of early osteoarthritis diagnosis and prognosis. *Therapeutic Advances in Musculoskeletal Disease, 28*(15), 1–12. https://doi.org/10.1177/1759720X231165560.

Morris, J., Roderick, P., Harris, S., Yao, G., Crowe, S., Phillips, D., Duncan, P., Fraser, S. (2021). Treatment burden for patients with multimorbidity: cross-sectional study with exploration of a single-item measure. *British Journal of General Practice, 71*(706), e381-e390. https://doi.org/10.3399/BJGP.2020.0883.

Nayak, U., Balachandra, M., Manjunath, K., Kurady, R. (2021). Validation of segmented brain tumor from MRI images using 3D printing. *Asian Pacific Journal of Cancer Prevention, 22*(2), 523-530. https://doi.org/10.31557/APJCP.2021.22.2.523.

Nolden, M., Zelzer, S., Seitel, A., Wald, D., Muller, M., Franz, A., Maleike, D., Fangerau, M., Baumhauer, M., Maier-Hein, L., Meinzer, H.-P., Wolf, I. (2013). The medical imaging interaction toolkit: challenges and advances: 10 years of open-source development. *International Journal of Computer Assisted Radiology and Surgery, 8*(4), 607-620. https://doi.org/10.1007/s11548-013-0840-8.

Palumbo, L., Bosco, P., Fantacci, M., Ferrari, E., Oliva, P., Spera, G., Retico, A. (2019). Evaluation of the intra- and inter-method agreement of brain MRI segmentation software packages: a comparison between SPM12 and FreeSurfer v6.0. *Physica Medica, 64*, 261–272. https://doi.org/10.1016/j.ejmp.2019.07.017.

Paproki, A., Engstrom, C., Strudwick, M., Wilson, K., Surowiec, R., Ho, C., Crozier, S., Fripp, J. (2017). Automated T2-mapping of the menisci from magnetic resonance images in patients with acute knee injury. *Academic Radiology, 24*(10), 1266-1274. https://doi.org/10.1016/j.acra.2017.04.017.

Preukschas, A., Wise, P., Bettscheider, L., Pfeiffer, M., Wagner, M., Huber, M., Golriz, M., Fischer, L., Mehrabi, A., Rossler, F., Speidel, S., Hackert, T., Muller-Stich, B., Nickel, F., Kenngott, H. (2024). Comparing a virtual reality head mounted display to on screen three-dimensional visualization and two-dimensional computed tomography for training in decision making in hepatic surgery: a randomized controlled study. *Surgical Endoscopy, 38*(5), 2483-2496. https://doi.org/10.1007/s00464-023-09989-9.

Rogelj, L., Dolenec, R., Tomšič, M., Laistler, E., Simončič, U., Milanič, M., Hren, R. (2022). Anatomically accurate, high-resolution modeling of the human index finger using in vivo magnetic resonance imaging. *Tomography, 8(*5), 2347-2359. https://doi.org/10.3390/tomography8050195.

Satava, R., Jones, S. (1998). Current and future applications of virtual reality for medicine. *Proceedings of the IEEE, 86*(3), 484-489. https://doi.org/10.1109/5.662875.

Scheys, L., Desloovere, K., Suetens, P., Jonkers, I. (2011). Level of subject-specific detail in musculoskeletal models affects hip moment arm length calculation during gait in pediatric subjects with increased femoral anteversion. *Journal of Biomechanics, 44*, 1346-1353. https://doi.org/10.1016/j.jbiomech.2011.02.074.

Smale, K., Conconi, M., Sancisi, N., Krogsgaard, M., Alkjaer, T., Parenti-Castelli, V., Benoit, D. (2019). Effect of implementing magnetic resonance imaging for participant-specific opensim models on lower-body kinematics and knee ligament lengths. *Journal of Biomechanics, 83*, 9-15. https://doi.org/10.1016/j.jbiomech.2018.11.029.

Tang, X., Guo, D., Liu, A., Wu, D., Liu, J., Xu, N., Qin, Y. (2022). Fully automatic knee joint segmentation and quantitative analysis for osteoarthritis from magnetic resonance (MR) images using a deep learning model. *Medical Science Monitor, 28*(10), e935496. https://doi.org/10.12659/MSM.935496.

Trimpl, M., Primakov, S., Lambin, P., Stride, E., Vallis, K., Gooding, M. (2022). Beyond automatic medical image segmentation - the spectrum between fully manual and fully automatic delineation. *Journal of Medical Engineering & Technology, 46*(7), 505-516. https://doi.org/10.1080/03091902.2022.2096550.

Zou, K., Warfield, S., Bharatha, A., Tempany, C., Kaus, M., Haker, S., Wells, W., Jolesz, F., Kikinis, R. (2004). Statistical validation of image segmentation quality based on a spatial overlap index. *Academic Radiology, 11*(2), 178–189. https://doi.org/10.1016/S1076-6332(03)00671-8.

Chapter 3: MANUSCRIPT 2

MRI-based Participant-specific vs. Generic Musculoskeletal Models: Effects on Marker Fit, Flexion Kinematics, and Participant-Level Patterns

Elese St Louis [1], Allison Clouthier [2], Karine Stoelben[3], Sasha Carsen [3], and Daniel L. Benoit [4]

[1] Faculty of Engineering, University of Ottawa, Canada
[2] School of Human Kinetics, University of Ottawa, Canada
[3] Division of Orthopaedics, Children's Hospital of Eastern Ontario, Canada
[4] Faculty of Medicine, Lund University, Sweden

Abstract

This study investigates whether incorporating MRI-based participant-specific tibia and femur geometries into musculoskeletal (MSK) models meaningfully alters biomechanical outputs in adolescent females with anterior cruciate ligament injuries. Thirty-one participants provided motion capture of a forward injured-leg leading lunge and MRI images to generate partial participant-specific knee joint geometries. Two validated MSK models (*Rajagopal* vs. *Catelli*) were modified using rigid and non-rigid registration followed by integration of the bone geometry via the *STAPLE* pipeline and scaling with the Automatic Scaling Tool. Model outputs were evaluated across three domains: (1) knee joint center (KJC) location, (2) knee flexion angle kinematics, and (3) marker trajectory error. KJC excursions were compared using repeated measures ANOVA across model types and preparation stages. Knee flexion angles were compared using statistical parametric mapping with two-way repeated measures ANOVA and further explored with participant-level root mean square (RMS) differences and Pearson correlations. Marker error was assessed using a nonparametric aligned rank test, and absolute differences in RMS error were examined descriptively.

Across all comparisons, participant-specific models produced results that were similar to generic models. Inconsequential KJC shifts (< 0.06 mm) led to no significant differences in knee flexion angles observed across models ($p > 0.05$). Participant-Specific *Rajagopal* vs. Participant-Specific *Catelli* showed differences in marker RMS error ($p < 0.001$), but absolute differences remained below clinically meaningful thresholds (< 0.25 mm). Most participants exhibited high waveform similarity between generic and participant-specific models ($RMS \leq 5°$, $r \geq 0.95$).

In conclusion, incorporating partial participant-specific bone geometry produced results that were highly consistent with generic models across knee joint center location, knee flexion kinematics, and marker trajectory errors. These findings suggest that the biomechanical impact of participant-specific modelling may not depend only on the type of anatomical personalization, but how that personalization is defined and integrated into the model.

3.1 Introduction

Musculoskeletal (MSK) models are powerful tools used to non-invasively simulate joint biomechanics and estimate internal forces that are otherwise impractical or unethical to measure in vivo. As such, these MSK models have gained relevance in clinical and research contexts related to rehabilitation planning, surgical intervention prediction, and injury prevention (Zhang et al., 2024; Thuraisingam et al., 2022; Kim et al., 2024).

OpenSim (SimTK.org; v4.4) is a widely used, open-source platform for developing and analyzing MSK models (Delp et al., 2007). It provides a flexible framework to simulate joint kinematics, estimate internal forces, and visualize musculoskeletal function during trials. From *OpenSim*, several MSK models have been developed and are available through the *OpenSim* project repository, each having varying levels of complexity and designed for different areas of interest. Among these generic models are the *Rajagopal* and *Catelli* models. The *Rajagopal* model was designed for young, healthy populations and provides a robust framework for simulating lower limb joint mechanics (*Rajagopal* et al., 2016). The *Catelli* model builds directly on this framework, retaining the joint structure with refinements to musculature to improve simulations at high-flexion joint angles (*Catelli* et al., 2019). For applications involving inverse kinematics, both models share a functionally equivalent structure allowing for direct comparison of geometry modifications without introducing differences from model or coordinate systems.

To adapt generic models to individual subjects, personalization is commonly achieved by scaling the model based on body segment dimensions and motion capture markers. However, more advanced personalization approaches have explored incorporating subject-specific bone geometries derived from medical imaging, such as computed tomography or magnetic resonance imaging (MRI). These geometries can be incorporated into full-body MSK models using tools like the Shared Tools for Automatic Personalized Lower Extremity Modelling (*STAPLE*) pipeline. *STAPLE* automates key steps such as aligning segmented geometries to the model, and updating associated dependencies (e.g., joints, markers, and muscles), while seeking to preserve original joint kinematics (Modenese et al., 2021).

Personalization in MSK models can occur at multiple levels to better reflect subject-specific anatomy and/or function. Among the options is personalizing bone geometry which can impact estimated joint kinematics, ligament loading, and contact forces (Martelli et al., 2015, Charles et al., 2021, Kainz et al., 2020). Changes to bone geometry often necessitate concomitant adjustments to nearby model structures, like muscle attachment sites; however, the studies that also adapt muscle volumes or tissue properties to match the anatomy result in personalization that is rarely limited to bone geometry alone. While these concomitant changes are reasonable, the changes make it difficult to isolate the specific influence of bone geometry on simulation outcomes.

In pediatric models, bone personalization may be particularly important due to ongoing growth and substantial variation in skeletal morphology. The generic models developed from adult data may not accurately represent these anatomical differences which can influence more nuanced simulation outcomes (Arnold et al., 2010). Addressing whether personalized bone geometries alone, without adjusting other aspects of the model, would help determine the minimum level of anatomical fidelity required to achieve biofidelic results in adolescent clinical populations.

The value of model personalization is open for debate. Some studies report improvements in biomechanical outputs, such as ligament strain or joint kinematics while using participant-specific geometries and joint definitions (Smale et al., 2019, Miller et al., 2023). Others, conversely, suggest that personalization has limited impact depending on the level of personalization carried out, or if changes are minimal. For example, Martelli et al. (2015) found that small changes in joint

axis definition caused only small variations (0.33 BW in joint forces) in MSK simulation results, and Roelker et al. (2017) showed that differences between generic models themselves, as defined in their creation, had more impact on joint moments than anatomical personalization might provide. These mixed findings highlight the need to better understand when and where personalization adds value.

The purpose of this study was therefore to examine whether incorporating participant-specific tibia and femur bone geometries, limited to distal and proximal regions of the tibiofemoral joint, would meaningfully influence biomechanical outputs in MSK models. Specifically, three outcome variables were investigated: (1) changes in knee joint center (KJC) determinant's location, (2) alterations in knee flexion angle trajectories, and (3) differences in marker trajectory fitting error. Specifically, these outcomes were assessed across model types (*Rajagopal* vs. *Catelli*), geometry specificity (Generic vs. Patient Specific), and through the participant-specific model creation stages (post-*STAPLE* vs. post-Automatic Scaling Tool (AST)). Therefore, this study seeks to isolate the effect of bone geometry personalization, without any additional model adaptations, on key simulation outputs during a functional task in adolescent ACL-injured participants. It was hypothesized that incorporating partial participant-specific geometry would result in minor shifts in KJC and marker error, but not enough to meaningfully alter knee flexion kinematics.

3.2 Materials and Methods

This retrospective, observational study utilized existing motion capture and imaging data from a larger ongoing prospective cross-sectional cohort study. Ethical approval was obtained from the Children's Hospital of Eastern Ontario (17/74X), and the University of Ottawa (H091710). A total of 31 female pediatric participants (age: 15.4 ± 1.2 yrs; height: 165.6 ± 5.3 cm; mass: 64.1 ± 8.3 kg) were selected from an ongoing longitudinal study on a pre- and post- reconstruction for an ACL injured population. Only participants with MRI-segmented bone geometries and those who completed lunge trials with the injured leg leading, (18 – left; 15 – right), were included.

3.2.1 Data Collection

3.2.1.1 Motion Data

All marker motion trajectories were collected using a 10-camera infrared motion analysis system (8 Vero; 2 Vantage, *VICON*, Oxford, UK) at 200 Hz and recorded using supported software (Nexus v2.7, *VICON*, Oxford, UK). Eighty-four retroreflective markers were placed on anatomical landmarks based on a modified UOMAM marker set (Mantovani et al., 2017), including anatomical and cluster markers of total body (Figure 3.1).

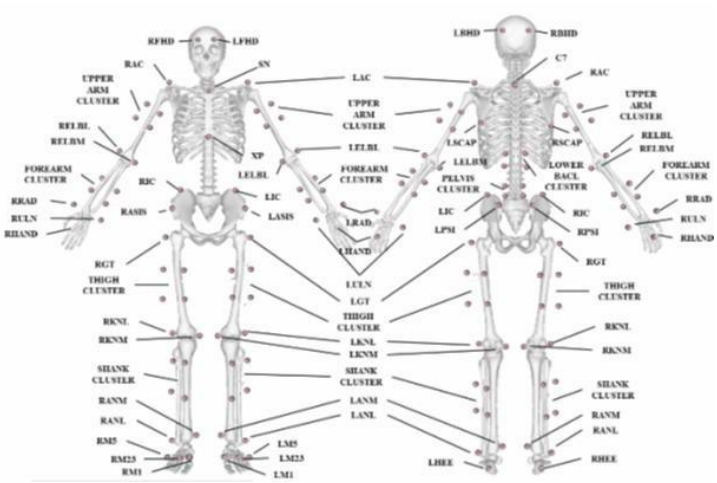

Figure 3.1: Clinical Biomechanics Research Unit's Custom Marker Placement for VICON retroreflective markers

As part of the larger protocol, each participant completed five forward lunge trials, stepping forward with the injured leg leading. Only the leading leg's eccentric portion of the lunge was analyzed. In this context, eccentric refers to the descent phase of the movement, defined as the period from the onset of forward motion to the point of global peak knee flexion. This definition is based on joint kinematics and does not imply specific muscle activation patterns, as cautioned by Jönhagen et al. (2009).

Marker trajectories were filtered using a 4th order zero-lag low-pass Butterworth filter with a cutoff frequency of 15 Hz using custom *VICON* pipelines scripts. A 20 Hz cutoff when sampled at 200 Hz is appropriate for high-velocity movements, so a more conservative 15 Hz cutoff was chosen to minimize noise while retaining key movement dynamics in the functional lunge task (Bisseling et al., 2006). In order to align reference systems with *OpenSim*, marker trajectories were rotated -90° about the global x-axis.

3.2.1.2 Imaging and Bone Meshes

3D geometries of the distal femur and proximal tibia were generated via *Elucis* (RealizeMedical, Ottawa, Canada) from magnetic-resonance imaging. Imaging parameters included a slice thickness of 3.0 - 3.5 mm, interslice gap of 0.3 - 1.0 mm, and field of view extending ± 150 mm from the tibiofemoral joint space. Only sagittal proton density Cube (SAG PD Cube) sequences were used for segmentation. Mesh refinement, which included removing non-manifold edges, holes, and duplicate faces/vertices, post-export of geometries, was performed in MeshLab (2023.12, Italy) to ensure structural integrity prior to further use in model creation. These methods led to a Dice similarity coefficient (DSC) of 0.90 for the femur, based on prior validation work comparing *Elucis* against a standard 2D segmentation tool (Medical imaging interaction toolkit; *MITK*) in pediatric knee MRI datasets (see Chapter 2). As the present study focused exclusively on bone structures, the high DSC achieved for the femur supports the use of *Elucis* for generating subject-specific bone geometries.

3.2.2 Musculoskeletal Modelling

3.2.2.1 Generic Models

The structurally similar *Rajagopal* et al. (2016) and *Catelli* et al. (2019) lower limb musculoskeletal models were used to evaluate the participant-specific pipeline. The *Rajagopal* model remains one of the most widely used full-body models for lower limb research (*Rajagopal*

et al., 2016) and the *Catelli* model adapted this model, building on Lai et al. (2017), with muscle paths to enhance simulations (*Catelli* et al., 2019). Both models include 20 degrees of freedom (DOF) in the lower body (six for pelvis, seven per leg). In both models, the knee joint is defined as a single-DOF joint, where tibial motion relative to the femur is governed by flexion-extension about the femur's fixed negative-Z axis. All other tibiofemoral motions (e.g., anterior-posterior translation, axial rotation) were parametrized as functions of the flexion angle using equations from Walker et al. (1988), with additional refinements to anterior-posterior translations after 60° of flexion in the *Catelli* model via Lai et al. (2017). From these changes, the *Rajagopal* model supports knee flexion up to 120°, while the *Catelli* model extends this to 145°. Consequently, only knee flexion angles were estimated using inverse kinematics, and all other joint motions of the knee were prescribed. As both models retain the same joint DOFs and segment definitions, direct comparison of knee flexion outputs is appropriate. All models were stripped of upper limb segments and associated dependencies to focus analysis on the lower limbs.

3.2.2.2 Participant-specific Bone Conformation

From the generic models, the generic geometries were used for the participant-specific conforming of the generic bone. Each participant-specific model had two bones, the tibia and femur, which underwent a two-stage alignment: rigid registration to roughly align the bones, then non-rigid deformation to adapt the generic bone to the patient's bone. Only the distal femur and proximal tibia portions of the participant-specific bone were available from MRI data. The initial rigid alignment was performed using the Iterative Closest Point (ICP) algorithm from an open-source library: Open3D (Zhou et al., 2018). ICP was run for a maximum of 50 iterations, with convergence defined by relative RMSE change $< 1 \times 10^{-6}$ between successive iterations. The algorithm minimized the point-to-point distance between meshes, using a rigid transformation (rotation and translation only). Registration quality was evaluated using the root mean square error (RMSE) of closest point distances, with alignment considered acceptable when RMSE < 2mm, and through a visual inspection. As ICP requires similar scaling and rough alignment prior to use, a manual pre-alignment step to orient the meshes based on their bounding box was applied for smooth Open3D use. Open3D allowed alignment between the partial participant-specific bone to the generic bone while preserving shape characteristics (Figure 3.2).

(A): Post-Scaling, Pre-Manual Alignment (B): Post-Rigid ICP Alignment

Figure 3.2: Participant-specific Bone Conformation Using Rigid Alignment. (A) Generic (yellow) overlaid with participant-specific bone segments (blue) following scaling but prior to manual orientation. (B) Resulting alignment after rigid registration using Iterative Closest Point (ICP) algorithm via Open3D, preserving major anatomical landmarks.

Following this rigid alignment, non-rigid deformation was applied to conform the generic bone geometry to the participant-specific bone surface. This step used the Coherent Point Drift (CPD) algorithm (Myronenko & Song, 2010) implemented through the open-source PyCPD library (Kade, 2020). The CPD algorithm was chosen for its ability to preserve point correspondence and shape continuity while allowing flexible deformation as participant-specific bone had increased surface variation against the generic counterpart. A region of interest was required for smooth operation of CPD, defined by anatomical bounds of the participant-specific bone, and a parameter of smoothness ($\beta = 0.5$), and a limit of 100 iterations was used to ensure bone mesh integrity (Figure 3.3). Finally, the resulting mesh was visually and numerically validated using RMSE-based alignment metrics. Following this process, the participant-specific full bone mesh was post-processed, which included removing non-manifold edges, holes, and duplicate faces/vertices, in MeshLab (2023.12, Italy) to ensure structural integrity again.

A.1: Posterior View of Generic Full Bone

B.1: Posterior View of Participant Specific Full Bone Post - CPD

A.2: Anterior-Inferior View of Generic Articular Surface

B.2: Anterior-Inferior View of Participant Specific Articular Surface Post - CPD

Figure 3.3: Comparison of Generic and Post-Conformation Rajagopal, Femur Geometries. Posterior and Anterior-inferior views of the generic (left, yellow) and participant-specific post-conformation (right, blue) Rajagopal, femur

meshes. (A.1, A.2) Views of the generic full bone and articular surface. (B.1, B.2) Corresponding views of the participant-specific mesh after non-rigid conformation using Coherent Point Drift (CPD) showing preservation of global morphology and increased anatomical fidelity at articular region.

3.2.2.3 Participant-specific Model Preparation

Participant-specific geometries were put into the generic musculoskeletal model using a modified pipeline – Shared Tools for Automatic Personalized Lower Extremity Modelling (*STAPLE*) (Modenese et al, 2016). *STAPLE* was used through the *OpenSim* 4.4 API for MatLab (R2024a, Massachusetts, US). This process allowed the tibia and femur mesh to be replaced with the aligned participant-specific geometries. All dependencies to these model geometries/bodies, such as 'JointSet', 'MarkerSet', 'MuscleSet', and 'WrapObjectSet', were updated to reference the new geometry bounds.

To update these spatial definitions of joints and attachments, the centroid shift of the participant-specific geometry was found between the generic and participant-specific bone surfaces. This determined shift was then applied to the corresponding 'PhysicalOffsetFrame' of the replaced bones within the joint definitions. To safeguard against unrealistic repositioning, a maximum shift upper bound of 2 cm was defined. This value was not expected to be reached but was chosen as a conservative threshold to flag potential misalignment. Prior work has reported joint center shifts of approximately 6.1 ± 2 mm across different personalization pipelines (Princelle et al., 2023), and Holden et al. (1998) applied perturbations within a 10 mm range when modifying joint center positions. Based on these references, the generous 2 cm limit was chosen as a warning against unrealistic positioning. The actual 'PathPoint' locations for muscles were also updated using this centroid shift approach. As real-time recalculation by *OpenSim* API tended to result in runtime errors, these 'PathPoint' locations were indirectly updated to avoid this through editing the *OpenSim* (.osim) XML files.

3.2.2.4 Model Scaling

All musculoskeletal models were scaled using the Automatic Scaling Tool (AST), which automates the process of aligning virtual model markers to experimentally captured marker locations, replacing the need for manual adjustments by the researcher (Di Pietro et al., 2024). Only anatomical markers were used during scaling. Marker weights were assigned based on their anatomical reliability and influence on model dimensions, so key bony landmarks (e.g., anterior superior iliac spine (ASIS), femoral epicondyles, malleoli) were assigned a higher weight of 20, while less critical markers were weighted at 1. This ensured accurate scaling near regions of interest while minimizing the influence of less stable surface markers. A uniform multiple marker-pair measurement set was applied across the feet, shank, thigh, pelvis, and torso segments. Arm markers were excluded from all models as any bodies on the arms or their dependencies have been previously removed.

As explained, in the AST framework, participant height and weight were used to determine an average scale factor to prevent unrealistic segment scaling factors from the uniform marker-pair measurement set. Parameters for AST were (1) Maximum of 400 iterations, (2) root mean square marker error fell below 1.0 mm, and/or (3) maximum marker error dropped below 2.5 mm. If the maximum number of iterations was reached, the model was run another time until the conditions were met.

3.2.2.5 Knee Joint Center

To evaluate how different stages of the modelling pipeline affect the estimated knee joint center, the positions of the femur and tibia reference frames (offset frames) were analyzed across three key stages. The femur and tibia offset frames were taken at the (1) generic for baseline, (2) post-*STAPLE* for bone conformation changes, and (3) post-AST for scaling changes. Euclidean distance differences were found between stages to determine shifts caused by these stages. Comparisons were performed separately for *Rajagopal* and *Catelli* models, while the generic models were excluded as there was no *STAPLE* stage.

3.2.3 Inverse Kinematics

Using the *OpenSim* 4.4 API in MatLab, inverse kinematics was used to estimate joint angles and evaluate marker trajectory error for each lunge trial. Four models were analyzed per participant (Generic and Participant-specific; *Rajagopal* and *Catelli*) and all trials with the injured leg leading were processed. Both anatomical and cluster markers were used during IK to ensure segment tracking while key anatomical landmarks were assigned higher weights, and cluster/less critical markers were set at a weight of 1. This weighting was designed to guide the IK solution toward physiological movement without overfitting to soft tissue artifact. Knee flexion angles and marker error during the lunge were the outputs of each trial.

3.2.3.1 Lunge Trial Normalization

To enable consistent comparison of lunge trials, the eccentric phase of the lunge (from movement onset to global peak knee flexion) was analyzed, as many participants lacked a complete concentric phase. Trials were then temporally aligned based on characteristic early peak in the eccentric phase and subsequently normalized to 101 points. This ensured standardized input for downstream comparisons across models and participants.

Finally, for each model and participant, a single representative trial was selected to maintain consistency across comparisons. Only lunge trials with a complete eccentric phase were considered valid and included in this selection process. This was done by first averaging all valid lunge trials for a given condition and then selecting the individual trial that had the lowest root mean square error (RMSE) relative to that average. This method ensured that the chosen trial reflected typical participant movement. Dynamic time warping was not entertained as it non-linearly alters the time axis of each waveform, violating assumptions required for statistical parametric mapping (SPM). Instead, trials were normalized using a procedure that preserves biomechanical interpretability while supporting valid SPM-based inferences.

3.2.4 Statistical Analysis

The following comparisons were made across models via SPSS (V29.0.2.0, Armonk, NY, US) unless otherwise stated. A total of 31 participants were included in all statistical analyses reflecting the complete subset of individuals in the longitudinal study that had segmented MRI geometries, and valid lunge trials with the injured leg leading.

3.2.4.1 Knee Joint Center Comparison

A repeated measures ANOVA was performed with stage (*STAPLE* vs. AST) and model type (*Rajagopal* vs. *Catelli*) as within-subject factors. Analyses of the femur and tibia offsets were conducted separately. Significance was set at $p < 0.05$.

3.2.4.2 Knee Flexion Angles – SPM ANOVA

Statistical parametric mapping (SPM) was used to compare knee flexion angles across models using the *spm1d* toolbox (v0.4) in MatLab (2024a, Massachusetts, US). A two-way repeated

measures SPM ANOVA was done with model type (*Rajagopal* vs. *Catelli*) and geometry specificity (Generic vs. Patient Specific) as within-subject factors. Significance was set as clusters where SPM(t) or SPM(F) exceeded the critical threshold (F*) at $\alpha = 0.05$, corrected for temporal smoothness.

3.2.4.2.1 Knee Flexion Waveform Similarity – RMS and Pearson Correlation

To further explore participant-level differences in knee flexion kinematics between generic and participant-specific models, an exploratory descriptive analysis was conducted. This analysis complements the SPM results by examining individual waveform agreement, with the goal of identifying model-specific inconsistencies or participant-specific response patterns that may be masked in group-level statistics.

For each participant, waveform similarity between the generic and participant-specific models was assessed using two metrics: (1) root mean square (RMS) difference, to quantify pointwise differences in knee flexion angle (in degrees), and (2) Pearson correlation coefficient (r), to measure the similarity in waveform shape. These metrics were used to characterize differences in amplitude (via RMS) and shape agreement (via r).

Participants were classified as high responders to geometric personalization if their RMS exceeded 5° and/or their correlation coefficient was below 0.95. A threshold of 5° RMS was used to indicate clinically meaningful angular deviation, consistent with prior validation studies showing that joint angle errors exceeding 5° may compromise clinical interpretation (Hu et al., 2022; McGinley et al., 2009). This value also aligns with biomechanical validation criteria from wearable sensor studies, which defines errors < 5° as acceptable for knee kinematics (Bessone et al., 2019). A correlation threshold of 0.95 was selected based on prior rehabilitation biomechanics research demonstrating that knee flexion waveform agreement in lunge and squat tasks is typically considered excellent at or above this level (Hu et al., 2022).

3.2.4.4 Marker Trajectory Errors

Mean RMS marker error was analyzed to evaluate the effects of model type (Rajagopal vs. Catelli) and geometry specificity (Generic vs. Participant-specific). A two-way repeated measures ANOVA was planned to test for main effects of model and specificity as well as their interaction. Normality was first assessed; if the assumption of normality was violated, a nonparametric aligned rank transform was used as an alternative for the 2x2 repeated-measures design. Significance was set at $p < 0.05$ and RMS values were interpreted relative to *OpenSim*'s best practice threshold of < 2 cm RMS marker error (Delp et al., 2012). Where significant effects were identified, differences between groups were further examined descriptively to assess biomechanical relevance. Specifically, individual-level absolute differences in mean RMS marker error were inspected within each significant comparison group.

3.3 Results

3.3.1 Knee Joint Center Comparisons – ANOVA

On average, the *STAPLE* stage caused a mean shift of 0.40 ± 0.00 mm for the femur and 0.39 ± 0.00 mm for the tibia across both models (*Rajagopal* and *Catelli*). In the AST stage, a smaller mean shift for the tibia, 0.03 ± 0.01 mm, was seen across both models, while the femur for the *Catelli* model was 0.03 ± 0.01 mm and for the *Rajagopal* model was 0.03 ± 0.01 mm. No significance was found between the model preparation stages and model type, yet significance was

found between *STAPLE* to AST stages ($p < 0.05$). The largest joint center shifts were found in three participants with peak displacements of 0.06 mm.

3.3.2 Knee Flexion Angles – SPM

No significant main effects or interactions were observed from the two-way repeated measures SPM ANOVA comparing model type and geometry as the SPM(F) values never exceeded the critical threshold ($F^* = 9.039$) (Figure 3.4).

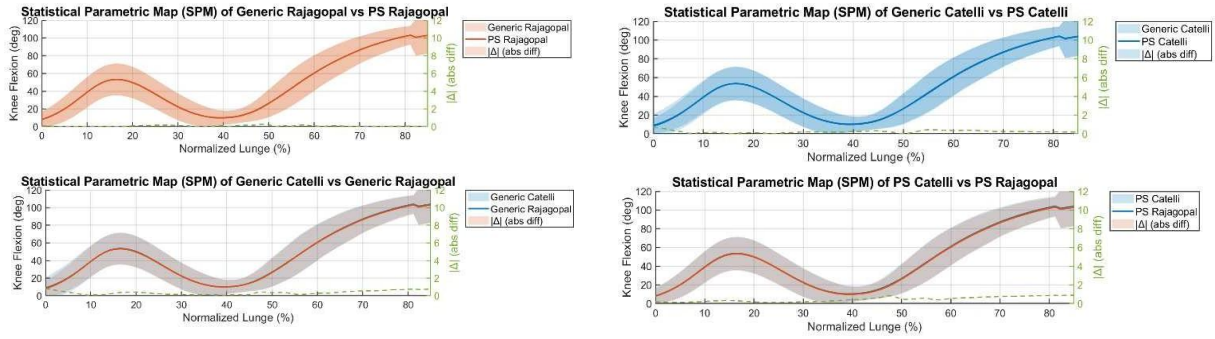

Figure 3.4: Knee flexion angle comparisons between model during the eccentric phase of the lunge. Mean ± standard deviation is shown for each model with shaded regions representing variability across participants. The dashed green line is the point-by-point absolute difference in knee flexion angle between models, which is quantified by the right-hand axis. Knee flexion values are time normalized across the lunge phase as 0-100% of lunge.

3.3.3 Waveform Similarity – RMS and Pearson Correlation

Most participants showed a high level of similarity (mean RMS difference ≤ 5°, mean r ≥ 0.95). Any high responders were classified as participants with RMS > 5 ° and/or r < 0.95. Three participants (9.7%) met this criterion, and all three were from the *Catelli* model comparison (Figure 3.5).

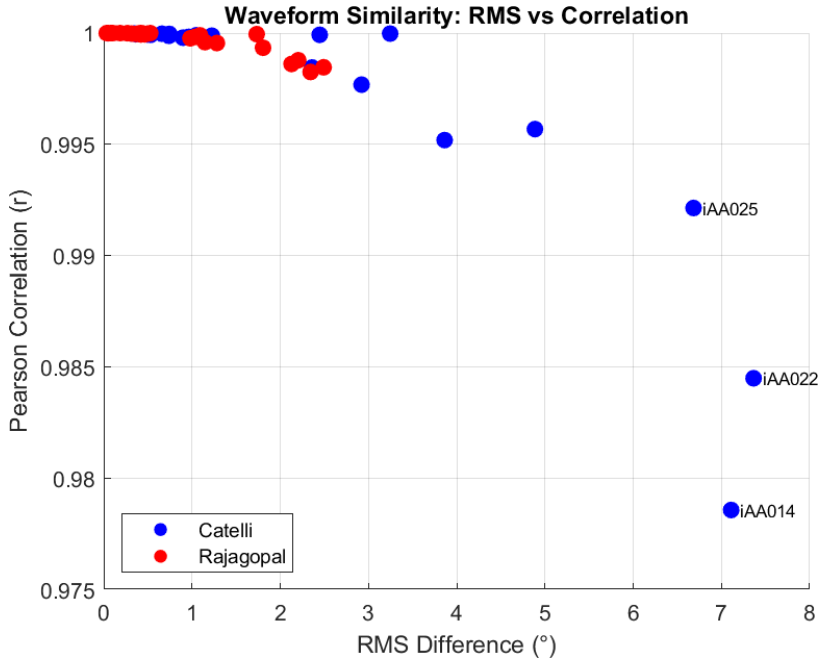

Figure 3.5: Waveform similarity between generic and participant-specific models for knee flexion through RMS difference versus Pearson correlation. Participants with high waveform similarity (RMS ≤ 5°, r ≥ 0.95) are shown as

only solid circles, while participants flagged as high responders (RMS > 5 °, r < 0.95) are labelled with their participant ID. Blue and red labels indicate Catelli and Rajagopal respectively.

3.3.4 Marker Trajectory Errors – Aligned Rank Test and Descriptive

The analysis of mean RMS marker error revealed a significant main effect of model type, ($F(1, 122) = 11.73$, $p < 0.001$), indicating differences in tracking performance between the Rajagopal and Catelli models. No significant main effect of geometry specificity was observed, ($F(1, 122) = 0.24$, $p = 0.625$)), and there was no significant model x specificity interaction ($F(1, 120) = 0.50$, $p = 0.48$).

To further inspect the significant model effect, descriptive comparisons were examined. Participant-specific Rajagopal vs. participant-specific Catelli conditions showed consistently lower RMS marker error for the Catelli model. Across all conditions, mean RMS marker errors ranged between 1-2.5 cm. Although statistically significant, the absolute differences between models were small, with typical participant-level deviations below 0.25 mm, remaining well within OpenSim's recommended < 2 cm RMS marker error threshold (Delp et al., 2012)

3.4 Discussion

This study aimed to assess how participant-specific bone geometries may influence musculoskeletal model outputs compared to generic models, using two structurally similar modelling frameworks (*Rajagopal* and *Catelli*). Across all analyses participant-specific models closely mimicked generic model frameworks, resulting in minor differences in knee joint center location, knee flexion kinematics, and marker trajectory errors. Although the Catelli model has an extended knee flexion capacity (145°) relative to the Rajagopal model (120°), the forward lunge task did not require participants to approach maximal knee flexion. As all trials remained below 120°, knee flexion stayed within the range supported by both models, likely contributing to the high agreement observed between models. While the *Catelli* model incorporates additional refinements to tibiofemoral translations at higher flexion angles (Lai et al., 2017), these modifications are not expected to influence the flexion-angle outputs evaluated in this study. However, as secondary joint motions are prescribed as coupled functions of flexion, minor influences on marker trajectory errors cannot be entirely excluded. While statistical significance for marker error was observed between Participant-specific *Rajagopal* vs. Participant-specific *Catelli*, the absolute difference was small enough to be considered below thresholds for biomechanical relevance.

Surprisingly, despite incorporating anatomically different geometry, participant-specific models produced similar results to their generic counterparts, with any changes well below known thresholds for biomechanical relevance. Prior literature suggests that generic MSK models may not fully capture the anatomical or functional characteristic of specific populations, especially in pediatric contexts. For instance, in pediatric cohorts, MRI-informed pipelines have been shown to significantly improve joint center estimation accuracy, while linearly scaled *OpenSim* models have performed poorly (Davico et al., 2020). Also, for knee joint mechanics, Martelli et al. (2015) demonstrated that uncertainty in defining joint axes, even when using subject-specific femur and tibia geometries, led to knee flexion angle variations of up to 5° in the sagittal plane, which highlights that seemingly small deviations in anatomical definition can influence knee kinematics.

This unexpected consistency, with this study, brings forth two important considerations: (1) the limited extent of bone replacement (partial femur and tibia) which served to minimize the influence of the participant-specific geometry on joint and movement calculations, and (2) the participant-specific model creation pipeline maintained biomechanical fidelity to the original

model structures. This suggests that partial personalization, limited to distal femur and proximal tibia, may be insufficient to meaningfully impact sagittal plane knee joint angles or marker trajectories, at least during controlled functional trials like the lunge. Altogether, our results suggest that the model preparation approach was robust, preserving intended joint definitions and movement behaviours even with the addition of participant-specific geometry.

3.4.1 Knee Joint Center Shifts

The extremely small joint center shifts observed between the *STAPLE* and AST stages offer insights into the pipeline's performance. Although both preparation stages were intended to modify the musculoskeletal models, the joint center changes were less than 0.006 mm. Prior work has shown that joint center changes up to 2.5 mm do not meaningfully affect model outputs such forces (Martelli et al., 2015), and other automated modelling pipelines have shown that while joint center shifts did have an effect, the impact was likely observed by other sources of uncertainty, including model assumptions and inter-operator variability (Modenese & Kohout, 2021). Therefore, the negligible shifts produced in this study would not be expected to affect joint kinematics, kinetics, and model performance. An important consideration for these minimal shifts is that only partial segments of the femur and tibia were replaced with participant-specific geometries. Since the entire morphology of the generic bone was not altered, the centroid of the re-mapped participant-specific bone remained close to the original centroid of the generic bone. This close spatial relationship is critical for the updated model elements, such as knee joint center, as these updates are based on the centroid shift between the generic and participant-specific bones during *STAPLE*. Thus, it can be concluded from this dataset that small morphological changes led to only slight adjustments to the biomechanical dependencies in the model. Given that centroid calculations, based on the centroid shift method, are sensitive to overall bone shape and extent, it is reasonable to assume a full-bone reconstruction would produce larger differences between generic and participant-specific geometries compared to only partial segments. This would likely produce larger shifts in estimated joint center locations, and then more pronounced changes in musculoskeletal model outputs, particularly for kinematic variables derived from joint definitions. In this study, joint centers were updated using a global alignment approach (centroid shift method), where transformations were based on the centroid change between the generic and participant-specific bones. This method was selected for its high level of automation and reproducibility, which are particularly advantageous when processing medium-to-large datasets; however, while the centroid shift method was able to preserve overall model integrity, the minimal differences observed between participant-specific and generic model outputs suggest that this global approach may not have been sensitive enough to capture individualized joint morphology, particularly given that only partial geometries were used. Alternate joint definition strategies using local geometry fitting, such as the GIBOC and Kai algorithms, define the joint center from anatomical landmarks like the femoral condyles or tibial plateau using shape fitting (Modenese et al., 2018; Kai et al., 2014). These techniques emphasize articular surface geometry rather than global mass distribution and may be more effective in extracting meaningful participant-specific variation. In fact, articulated shape models, which account for pose and shape variation across bones, have shown improved reconstruction accuracy from sparse landmarks particularly in pediatric populations (Zhang et al., 2016; Carman et al., 2024). So, based on the minimal impact observed in this study using the centroid-based alignment, future investigations would benefit from exploring more anatomically grounded approaches that prioritize local joint morphology to better leverage the available participant-specific data over global approaches.

Despite the non-significant findings, two key conclusions can be drawn from our results. First, the *STAPLE* stage, relative to the AST scaling stage, had a greater influence on joint center position. This suggests that the pipeline, even during subtle changes, allows personalized bone geometry to directly modify model structure without unintended distortion from the scaling process. Second, the preservation of the joint center locations across the full pipeline serves to validate that the participant-specific model creation pipeline did not introduce unintended biomechanical artifacts. Instead, any differences found between models can be attributed to the anatomical features of the bones themselves rather than pipeline-induced changes. This has important implications where participant-specific joint mechanics are critical, such as clinical decision-making or surgical planning, and it confirms that the personalization step (*STAPLE*) successfully integrates participant-specific anatomical variation which remains stable through subsequent scaling processes.

3.4.2 Knee Flexion Angles

Knee flexion angle comparison revealed no significant differences across model types (*Rajagopal* vs. *Catelli*) nor geometric specificity (Generic vs. Participant-specific) during the eccentric portion of the lunge. Across all four conditions, the SPM(F) values remaining below the critical threshold (F*) suggests that the use of the participant-specific tibia and femur geometries did not meaningfully alter the sagittal knee kinematics during this movement. This outcome continues to support the consistency of the participant-specific modelling pipeline along with the knee joint center data. Essentially, the models having nearly identical knee flexion outputs reinforce that the joint mechanics were preserved throughout the *STAPLE* and AST stages.

Further supporting these findings, high participant-level agreement occurred across generic and participant-specific knee flexion waveforms. RMS differences were consistently small ($\leq 5°$) and Pearson correlation coefficients were high (≥ 0.95) across most participants. Only three out of 31 participants were flagged as high responders, all within *Catelli* model comparisons. The generic bone geometries are shared between the *Catelli* and *Rajagopal* models, and the flexion-extension outputs are unaffected by the muscle wrapping surfaces added in *Catelli*; thus, these high individual responder cases may reflect factors unrelated to bone geometry or kinematic optimization, such as participant-specific movement variability or residual marker placement error. However, as secondary joint motions are prescribed as coupled functions of flexion, minor influences on marker trajectory errors specific to the Catelli model cannot be entirely excluded. Since all high responder cases occurred within the Catelli model comparisons, further investigation may be warranted to determine whether these kinematic coupling differences contribute to individual sensitivity in marker-based error metrics.

Our findings align with prior literature demonstrating that even with participant-specific geometries integrated using differing pipelines, if joint centers and axes were maintained, primary biomechanical outputs such as joint contact forces remained consistent (Princelle et al., 2023). In this study, only partial bone geometries (distal femur and proximal tibia) were updated, which likely limited the extent of introduced structural variation. As such, the resulting knee flexion outputs were expected and observed to remain consistent across models. This raises an important consideration about both the extent and type of personalization needed to meaningfully impact biomechanical outcomes.

It is important to acknowledge that this study focused exclusively on sagittal plane knee kinematics (flexion-extension), consistent with the single-DOF hinge constraint implemented in most OpenSim based knee models. While this simplification allowed for robust comparisons and efficient processing, it does not account for potential changes in other tibiofemoral-DOF (rotations

and translations). Prior work has shown that these secondary motions can be particularly sensitive to partially constrained motion, marker tracking errors, and joint definitions. For instance, Miller et al. (2023), using a partially constrained six DOF knee model, demonstrated that non-sagittal-DOFs, such as internal-external rotation, exhibited more pronounced group differences between ACL-injured and healthy participants than flexion-extension. This suggests that personalization strategies may have a greater impact when applied to DOFs beyond flexion, particularly in models that resolve joint kinematics more independently. However, accurately capturing these motions using traditional marker-based motion capture presents a challenge. Non-sagittal DOFs are notoriously prone to soft tissue artifact and joint observability limitations (Kozanek et al., 2009). For example, Benoit et al. (2006), reported that errors in internal-external rotation and abduction-adduction reached up to 13°, while errors in flexion-extension were limited to 2 - 3°. These findings suggest that non-sagittal DOF are not only prone to measurement error but also are more sensitive to joint definitions or how joint axes are defined.

By reporting only flexion-extension, which is solved independently while other DOFs were prescribed, this study may have masked subtler effects of bone personalization. Future studies would examine the effect of participant-specific bone geometry across all six DOF using decoupled, or partially constrained joint kinematics. This may provide a more complete understanding of how subject-specific anatomy influences multiplanar joint mechanics.

These findings reinforce the broader principle in the literature that not all personalization strategies contribute equally to all biomechanical outputs (Martelli et al., 2015; Valente et al., 2014). Personalizing bone surfaces, as done in this study, may have limited influences on joint kinematics but could be critical for other outputs, such as muscle leverage or ligament strain (Scheys et al., 2008; Smale et al., 2019). So, the choice of personalization needs to be aligned with the specific intended simulation outcomes. This highlights the importance of tailoring model personalization to the research question, such as full bone reconstructions or locally fitted geometries may be necessary when simulating joint loading of soft tissue strain.

3.4.3 Marker Trajectory Errors

The aligned rank transform analysis revealed that model type (*Rajagopal* v. *Catelli*) significantly influences marker RMS error, while geometry specificity (Generic v. Participant-Specific) did not. There was no interaction between model and specificity, suggesting that the effect of model choice was consistent across geometry types. Descriptive inspection of participant-level results showed that, although the *Catelli* model tended to produce lower RMS marker error than the *Rajagopal* model, absolute differences were small (< 0.25 mm across participants) and well below *OpenSim*'s accepted best-practice threshold of 20 mm (*OpenSim*, 2019), indicating that this is not biomechanically meaningful.

These findings reinforce that the participant-specific modelling pipeline maintained consistent and robust marker tracking performance across models. Small model-to-model differences are expected in personalized frameworks, particularly with changes to bone geometries and dependent markers, yet this study shows such differences were minor and unlikely to compromise simulation interpretation during functional movements like the forward lunge.

More importantly, this study's results support the validity of the Automatic Scaling Tool (AST) for scaling participant-specific musculoskeletal models. AST is a relatively recent development intended to automate the scaling process while still ensuring high-fidelity marker matching (Di Pietro et al., 2024). The absence of meaningful marker trajectory errors, along with the minor changes to kinematics and segment positioning, shows that AST successfully preserved critical anatomical relationships across models during scaling. Thus, beyond validating the broader

participant-specific modelling process, this study indicates that AST can be effectively applied in participant-specific modelling studies.

3.4.4 Limitations

Several limitations should be considered when interpreting these findings. First, MRIs only captured a limited region of the tibiofemoral joint (± 150 mm), preventing full-bone reconstruction. The use of full femur and tibia geometries may have produced larger effects on joint kinematics and marker trajectory error. Second, a key limitation of this study is that only knee flexion angles were independently estimated. The remaining tibiofemoral degrees of freedom were prescribed based on this flexion angle, as pre-defined by the joint kinematic coupling in these models. As such, the potential influence of participant-specific bone geometry on other aspects of joint motion (e.g., tibial translation, axial rotation) was not assessed. Third, all participants were female adolescents recovering from ACL injuries; generalizations to males or other age groups should made with caution. Third, only the eccentric phase of the forward lunge, on the injured leading leg, was analyzed. Results may not generalize to higher-impact, multi-planar tasks like cutting or jumping. Finally, soft tissue structures, such as ligaments, cartilage and menisci, were not modelled in this study. Future work should incorporate these structures to better capture complex joint behaviour and improve simulation fidelity.

3.5 Conclusion

Across all analyses, including knee joint center locations, knee flexion kinematics, and marker trajectory errors, results were highly consistent between model types (Generic vs. *Rajagopal*) and geometry specificity (Generic vs. Participant-specific). Although some comparisons reached statistical significance, all differences fell below established thresholds for biomechanical relevance. These outcomes reinforced the robustness of the participant-specific modelling pipeline and supports the validity of the Automatic Scaling Tool (AST) for scaling individualized models.

While the findings suggest that partial bone alone may not be sufficient for meaningful changes to joint kinematics during controlled movements like the forward lunge, they emphasize that model personalization should not be assumed to improve outcomes across all applications. The degree and type of personalization must carefully match the simulation goal and available participant-specific data.

3.6 References

Arnold, E., Ward, S., Lieber, R., Delp, S. (2010). A model of the lower limb for analysis of human movement. *Annals of Biomedical Engineering, 38*, 269-279. https://doi.org/10.1007/s10439-009-9852-5.

Benoit, D. L., Ramsey, D., Lamontagne, M., Xu, L., Wretenberg, P., Renström, P. (2006). Effect of skin movement on knee kinematics during gait and cutting motions measured in vivo. *Gait Posture, 24*(2), 152-164. tps://doi.org/j.gaitpost.2005.04.012

Besl, P., McKay, N. (1992). A method for registration of 3-D shapes. *IEEE Transactions on Pattern Analysis and Machine Intelligence, 14*(2), 239-256. https://doi.org/10.1109/34.121791.

Bessone, V., Höschele, N., Schwirtz, A., Seiberl, W. (2019). Validation of a new inertial measurement unit system based on different dynamic movements for future in-field applications. *Sports Biomechanics, 21*(6), 685-700. https://doi.org/10.1080/14763141.2019.1671486.

Bisseling, R., Hof, A. (2006). Handling of impact forces in inverse dynamics. *Journal of Biomechanics, 39*(13), 2438-2444. https://doi.org/10.1016/j.jbiomech.2005.07.021.

Carmen, L., Besier, T., Rooks, N., Choisne, J. (2024). An articulated shape model to predict paediatric lower limb bone geometry using sparse landmarks. *Journal of Biomechanics, 172*, 112211. https://doi.org/10.1016/j.jbiomech.2024.2024.112211.

Catelli, D., Wesseling, M., Jonkers, I., Lamontagne, M. (2019). A musculoskeletal model customized for squatting task. *Computer Methods in Biomechanics and Biomedical Engineering*, *22*(1), 21-24. https://doi.org/10.1080/10255842.2018.1523396.

Charles, J., Fu, F., Anderst, W. (2021). Predictions of anterior cruciate ligament dynamics from subject-specific musculoskeletal models and dynamic biplane radiography. *Journal of Biomechanical Engineering, 143*(3), 031006. https://doi.org/10.1115/1.4048710.

Davico, G., Pizzolato, C., Killen, B., Barzan, M., Suwarganda, E., Lloyd, D., Carty, C. (2020). Best methods and data to reconstruct paediatric lower limb bones for musculoskeletal modeling. *Biomechanics and Modeling in Mechanobiology, 19*(4), 1225-1238. https://doi.org/10.1007/s10237-019-01245-y.

Delp, S. L., Hicks, J. L., & Uchida, T. K. (2012). Best practices for scaling, inverse kinematics, and inverse dynamics in *OpenSim* [Workshop handout]. *SimTK*.

Delp, S., Anderson, F., Arnold, A., Loan, P., Habib, A., John, C., Guendelman, E., Thelen, D. (2007). *OpenSim*: Open-source software to create and analyze dynamic simulations of movement. *IEEE Transactions on Biomedical Engineering, 54*(11), 1940-1950. https://doi.org/10.1016/j.jbiomech.2020.110186.

Delp, S., Maloney, W. (1993). Effects of hip center location on the moment-generating capacity of the muscles. *Journal of Biomechanics, 26*(4), 485-499. https://doi.org/10.1016/0021-9290(93)90011-3.

Di Pietro, A., Bersani, A., Curreli, C., Di Puccio, F. (2024). AST: An *OpenSim*-based tool for the automatic scaling of generic musculoskeletal models. *Computers in Biology and Medicine, 175*, 108524. https://doi.org/10.1016/j.compbiomed.2024.108524.

Dranetz, J., Chen, S., Choi, H. (2024). Impact of model geometry and joint center locations on inverse kinematic/dynamic predictions: A comparative study of sexually dimorphic models. *Journal of Biomechanics, 169*, 112147. https://doi.org/10.1016/j.jbiomech.2024.112147.

Holden, J., Stanhope, S. (1998). The effect of variation in knee joint center location estimates on net knee joint moments. Gait & Posture, 7(1), 1-6. https://doi.org/10.1016/S0966-6362(97)00026-x.

Hu, G., Wang, W., Chen, B., Zhi, H., Li, Y., Shen, Y., Wang, K. (2021). Concurrent validity of evaluating knee kinematics using Kinect system during rehabilitation exercise. *Medicine in Novel Technology and Devices, 11*, 100068. https://doi.org/10.1016/j.medntd.2021.100068.

Jönhagen, S., Halvorsen, K., Benoit, D.L. (2009). Muscle activation and length changes during two lunge exercises: implications for rehabilitation. *Scandinavian Journal of Medicine & Science in Sports, 19*(4), 561-8. https://doi.org/10.1111/j.1600-0838.2007.00692.x.

Kade, S. (2020). PyCPD: Coherent point drift in python. *Github*. https://github.com/siavashk/pycpd

Kai, S., Armand, S., Bonnet, X., Remy-Neris, O., St-Onge, N. (2014). A comprehensive method for the estimation of anatomical frames orientation from three-dimensional bone geometries. *Journal of Biomechanics, 47*(5), 1229-1233. https://doi.org/10.1016/j.jbiomech.2013.12.013.

Kainz, H., Killen, B., Wesseling, M., Perez-Boerema, F., Pitto, L., Aznar, J., Shelfelbine, S., Jonkers, I. (2020). A multi-scale modeling framework combining musculoskeletal rigid-body simulations with adaptive finite element analyses, to evaluate the impact of femoral geometry on hip joint contact forces and femoral bone growth. *PLoS One, 15*(7), e0235966. https://doi.org/10.1371/journal.pone.0235966.

Kainz, H., Wesseling, M., Jonkers, I. (2021). Generic scaled versus subject-specific models for the calculation of musculoskeletal loading in cerebral palsy gait: Effect of personalized musculoskeletal geometry outweighs the effect of personalized neural control. *Clinical Biomechanics, 87*, 105402.https://doi.org/ 10.1016/j.clinbiomech.2021.105402.

Kim, S., So, J., Jeon, Y., Moon, J. (2024). Effect of changes in motor skill induced by educational video program to decrease lower-limb joint load during cutting maneuvers: based on musculoskeletal modeling. *BMC Musculoskeletal Disorders, 25*, 527. https://doi.org/10.1186/s12891-024-07642-4.

Kozanek, M., Hosseini, A., Liu, F., Van de Velde, S., Gill, T., Rubash, H., Li, G. (2009). Tibiofemoral kinematics and condylar motion during the stance phase of gait. *Journal of Biomechanics, 42*(12), 1877-1884. https://doi.org/10.1016/j.jbiomech.2009.05.003.

Lai, A., Arnold, A., Wakeling, J. (2017). Why are antagonist muscles co-activated in my simulation? A musculoskeletal model for analyzing human locomotor task. *Annals of Biomedical Engineering, 45*(12), 2762-2774. https://doi.org/10.1007/s10439-017-1920-7.

Mantovani, G., Lamontagne, M. (2017). How different marker sets affect joint angles in inverse kinematics framework. *Journal of Biomechanical Engineering, 139*(4). https://doi.org/10.1115/1.4034708.

Martelli, S., Valente, G., Viceconti, M., Taddei, F. (2015). Sensitivity of a subject-specific musculoskeletal model to the uncertainties on the joint axes location. *Computer Methods in Biomechanics and Biomedical Engineering*, 18(14), 1555-1563.https://doi.org/ 10.1080/10255842.2014.930134.

McGinley, J., Baker, R., Wolfe, R., Morris, M. (2009). The reliability of three-dimensional kinematic gait measurements: A systematic review. *Gait & Posture, 29*, 360-369. https://doi.org/10.1016/j.gaitpost.2008.09.003.

Miller, B. (2023). A participant-specific knee model driven by in vivo kinematics to better represent an ACL-injured pediatric population. (Master Thesis, University of Ottawa). pp. 86-101.

Miranda, D., Rainbow, M., Leventhal, E., Crisco, J., Fleming, B. (2010). Automatic determination of anatomical coordinate systems for three-dimensional bone models of the isolated human knee. *Journal of Biomechanics, 43*(8), 1623-1626. https://doi.org/10.1016/j.jbiomech.2010.01.020.

Modenese, L., & Kohout, J. (2020). Automated generation of three-dimensional complex muscle geometries for use in personalized musculoskeletal models. *Annals of Biomedical Engineering, 48*(12), 1793–1804.

Modenese, L., Ceseracciu, E., Reggiana, M., Lloyd, D. (2016). *STAPLE*: An open-source pipeline for the generation of subject-specific musculoskeletal models using *OpenSim*. *Computer Methods and Programs in Biomedicine, 124*, 99-110. https://doi.org/10.1016/j.cmpb.2015.10.014

Modenese, L., Renault, J., Weinert-Aplin, R. (2018). Automated generation of three-dimensional complex bone geometries and muscle paths for musculoskeletal modeling. *Journal of Biomechanics, 67*, 103-110. https://doi.org/10.1016/j.jbiomech.2017.12.004.

Modenese, L., Renault, J.-B., (2021). Automatic generation of personalized skeletal models of the lower limb from three-dimensional bone geometries. *Journal of Biomechanics, 116*, 110186. https://doi.org/10.1016/j.jbiomech.2020.110186.

Myer, G., Ford, K., Di Stasi, S., Barber, K., Micheli, L., Hewett, T. (2015). High knee abduction moments are common risk factors for patellofemoral pain (PFP) and anterior cruciate ligament (ACL) injury in girls: is PFP itself a predictor for subsequent ACL injury?. *British Journal of Sports Medicine, 49*(2), 118-122. https://doi.org/10.1136/bjsports-2013-092536.

Myronenko, A., Song, X. (2010). Point set registration: Coherent point drift. *IEEE Transactions on Pattern Analysis and Machine Intelligence, 32*(12), 2262-2275. https://doi.org/10.1109/TPAMI.2010.46.

OpenSim. (2019). Inverse Kinematics. *SimTK Confluence*. https://*OpenSim*confluence.atlassian.net/wiki/spaces/*OpenSim*/pages/53090037/Inverse+Kinematics

Powden, C., Hoch, J., Hoch, M. (2015). Reliability and minimal detectable change of the weight-bearing lunge test: A systematic review. *Manual Therapy, 20*, 524-532. https://doi.org/10.1016/j.math.2015.01.004.

Princelle, D., Davico, G., Viceconti, M. (2023). Comparative validation of two participant-specific modeling pipelines for predicting knee joint forces during level walking. *Journal of Biomechanics, 159*, 111758. https://doi.org/10.1016/j.jbiomech.2023.111758.

Rainbow, M., Miranda, D., Cheung, R., Schwartz, J., Crisco, J., Fleming, B., Davis, I. (2013). Automatic determination of an anatomical coordinate system for a three-dimensional model of the human patella. *Journal of Biomechanics, 46*(12), 2093-2096. https://doi.org/10.1016/j.jbiomech.2013.05.002.

Rajagopal, A., Dembia, C., DeMers, M., Delp, D., Hicks, J., Delp, S. (2016). Full-body musculoskeletal model for muscle-driven simulation of human gait. *IEEE Transactions on Biomedical Engineering, 63*(10), 2068-2079. https://doi.org/10.1109/TBME.2016.2586891.

Roelker, S., Caruthers, E., Baker, R., Vignes, G., Schultz, S., Chaudhari, A. (2017). Interpreting musculoskeletal models and dynamic simulations: Causes and effects of differences between models. *Annals of Biomedical Engineering, 45*(11), 2615-2627. https://doi.org/10.1007/s10439-017-1894-5.

Scheys, L., Van Campenhout, A., Spaepen, A., Suetens, P., Jonkers, I. (2008). Personalized MR-based musculoskeletal models compared to rescaled generic models in the presence of increased femoral anteversion: effect on hip moment arm lengths. *Gait Posture, 28*(3), 358-365. https://doi.org/10.1016/j.gaitpost.2008.05.002.

Smale, K., Conconi, M., Sancisi, N., Krogsgaard, M., Alkjaer, T., Parenti-Castelli, V., Benoit, D. (2019). Effect of implementing magnetic resonance imaging for participant-specific *OpenSim* models on lower-body kinematics and knee ligament lengths. *Journal of Biomechanics, 83*, 9-15. https://doi.org/10.1016/j.jbiomech.2018.11.016.

Thelen, D., Choi, K., Schmitz, A. (2014). Co-simulation of neuromuscular dynamics and knee mechanics during human walking. *Journal of Biomechanics, 136,* 1-8. https://doi.org/10.1115/1.4026358.

Thuraisingam, S., Chondros, P., Manski-Nankervis, J., Spelman, T., Choong, P., Gunn, J., Dowsey, M. (2022). Developing and internally validating a prediction model for total knee replacement surgery in patients with osteoarthritis. *Osteoarthritis and Cartilage Open, 4*(3), 100281. https://doi.org/10.1016/j.ocarto.2022.100281.

Valente, G., Pitto, L., Testi, D., Seth, A., Delp, S., Stagni, R., Viceconti, M., Taddei, F. (2014). Are subject-specific musculoskeletal models robust to the uncertainties in parameter identification?. *PLoS One, 9*(11), e112625. https://doi.org/10.1371/journal.pone.0112625.

Walker, P.S., Rovick, J.S., Robertson, D.D. (1988). The effects of knee brace hinge design and placement on joint mechanics. *Journal of Biomechanics, 21*(11), 965-974. https://doi.org/10.1016/0021-9290(88)90135-2.

Zhang, J., Besier, T. (2016). Accuracy of femur reconstruction from sparse geometric data using a statistical shape model. *Computer Methods in Biomechanics and Biomedical Engineering, 20(*5), 1-11. https://doi.org/10.1080/10255842.2016.1263301.

Zhang, L., Ma, R., Li, H., Wan, X., Xu, P., Zhu, A., Wei, P. (2024). Comparison of knee biomechanical characteristics during gait between patients with osteoarthritis and healthy individuals. *Heliyon, 10*(17), e36931. https://doi.org/10.1016/j.heliyon.2024.e36931.

Zhou, Q.-Y., Park, J., Koltun, V. (2018). Open3D: A modern library for 3D data processing. *arXiv preprint* arXiv:1801.09847. https://doi.org/10.48550/arXiv.1801.09847.

Chapter 4: General Discussion/Conclusion

4.1 Overview

This thesis aimed to evaluate two critical stages in development of participant-specific musculoskeletal (MSK) models surrounding the tibiofemoral joint: anatomical segmentation and biomechanical simulation. Study 1 compared the performance of *Elucis*, a virtual reality (VR) based segmentation tool, to *MITK*, a traditional 2D platform. Study 2 examined whether incorporating partial participant-specific bone geometries into *OpenSim* models meaningfully affected simulation outputs during a forward lunge. Together, these studies provide insight into both process efficiency and the biomechanical relevance of anatomical personalization in knee-specific MSK modelling pipelines.

4.2 Segmentation Efficiency

Results from Study 1 demonstrated that *Elucis* reduced segmentation time while maintaining or exceeding geometric agreement standards, particularly for smaller structures like the posterior cruciate ligament (PCL). These findings align with previous work emphasizing the challenge of segmenting small structures due to increased user variability and reduced anatomical contrast (Kway et al., 2021; Deeley et al., 2011; Fiederer et al., 2019). The PCL specifically is difficult to delineate using conventional 2D tools given its low T2-weighted signal and curved morphology (Johnston et al., 2018; Liimatainen et al., 2021).

The immersive interface of *Elucis* likely enhanced the spatial understanding and reduced reliance on anatomical interference, an issue with slice-by-slice segmentation (Preukschas et al., 2024; Satava et al., 1998). This improved reliability, particularly in novice users, supports growing evidence that VR-based tools can standardize workflows and reduce segmentation subjectivity (Hornsey et al., 2024; Preukschas et al., 2024). These results support *Elucis* as a viable, time-efficient alternative for creating personalized geometries.

4.3 Partial Personalization Impact for Simulations

Study 2 showed that replacing the distal femur and proximal tibia with participant-specific geometries had limited impact on simulation outputs. Differences in knee joint center location were negligible (< 0.006 mm), marker root-mean-square (RMS) error remained below *OpenSim*'s accepted threshold of 20 mm (*OpenSim*, 2019), and knee flexion angle waveforms were nearly identical across all model types.

This contrasts with prior studies that reported larger biomechanical differences following personalization, but those studies typically replaced full bone segments and incorporated other modifications such as personalized joint constraints or muscle definitions (Smale et al., 2019; Kainz et al., 2021). The limited personalization in this thesis, restricted to partial geometry alone, appears insufficient to meaningfully alter biomechanical outputs in constrained tasks like the forward lunge.

The negligible joint center shift observed in this study likely reflects the centroid-based realignment strategy used to update offset frames, where the femur and tibia were repositioned based on the shift between generic and participant-specific bone centroids. While this preserves overall bone positioning, it may reduce the influence of local anatomical differences, especially when only part of the bone surface is updated. Recent studies suggest that local geometry fitting,

such as articulated shape models or landmark-based reconstruction, may better capture these nuanced morphological variations in pediatric populations (Carmen et al., 2024; Zhang et al., 2016).

4.4 Leveraging Musculoskeletal Modelling Tools for Participant Specificity

Despite the lack of substantial differences in kinematics, this thesis highlights the strength of using existing modelling tools in a modular, task-specific way. The Automatic Scaling Tool (AST) was effective in preserving anatomical relationships and minimizing marker error during model scaling, even after manual geometry updates. Rigid and nonrigid alignment of bone geometries using iterative closest point (ICP) and coherent point drift (CPD) enabled the integration of participant-specific morphology without compromising the spatial integrity of the geometry. *STAPLE* was employed to generate and maintain functional joint coordinate systems and facilitate compatibility with *OpenSim* which offered a reliable structure on which customized updates could be applied. Overall, rather than relying on a single unified pipeline, this approach allowed existing tools to be flexibly adapted and combined to support participant-specific modelling in a way that suits the available data.

In pediatric contexts where full anatomical imaging is limited, modelling must balance practicality with fidelity, and this strategy offers a scalable and robust solution. While partial geometry updates alone may not strongly influence outputs like joint angles in constrained tasks, their inclusion allows for structural accuracy and positions the model for future refinement. For applications demanding greater sensitivity, such as modelling ligament strain, joint instability, or dynamic multi-planar tasks, more comprehensive personalization is enabled through anatomical exactness (Smale et al., 2019; Scheys et al., 2008; Charles et al., 2021).

4.5 Integration of Findings and Future Directions

These two studies were able to highlight key trade-offs between anatomical fidelity, simulation efficiency, and degree of personalization. Study 1 demonstrated that newer VR-based segmentation tools can reduce the time burden while improving user consistency, an important advancement in preparing participant-specific geometry for modelling. Then, Study 2 revealed that partial personalization of bone anatomy may not be sufficient to meaningfully alter simulation outputs during single-plane, controlled tasks.

These findings support a growing consensus that the degree and type of personalization should be aligned with the intended simulation goal (Martelli et al., 2015; Valente et al., 2014). For example, bone personalization may have limited impact on joint angles but may be critical when modelling ligament mechanics or musculoskeletal loading (Marieswaren et al., 2018). Therefore, future work should investigate whether certain personalization strategies, such as participant-specific bone alone, may have a greater influence on muscle forces, joint contact forces, or ligament loading. Similarly, tasks that demand multiplanar loading or instability, such as side-cutting or jump landing, may reveal differences not captured in forward lunge and should be explored too (Alkjaer et al., 2020; Comfort et al., 2015).

Future studies should examine different strategies for determining joint centers, particularly for global alignment methods (e.g., centroid shifts based on whole-mass distribution) versus local landmark-based fitting techniques. The current study used a global transformation to update joint centers which may have overlooked important articular geometry, especially when only using

partial geometries. Investigating how these approaches effect simulation outputs, especially across multiple DOF (e.g., internal-external rotation, varus-valgus angles or translational movements) and across different movement types, could provide further insight into personalization strategies. Also, expanding research beyond adolescent females with ACL injuries to include other age groups and injury types will also enhance generalizability and clinical relevance.

Finally, this thesis contributes to key stages of participant-specific knee MSK model development. These findings demonstrate that (1) VR-based segmentation tools like *Elucis* offers improved efficiency and inter-rater reliability, particularly for smaller structures, (2) partial personalization of bone geometry based on global registration is insufficient to meaningfully alter joint center, kinematics, or marker-based outcomes during forward lunges, and (3) the level of personalization on a model should be guided by the specific research question, not assumed to universally improve model outputs.

In sum, this work highlights the importance of aligning segmentation and personalization strategies with the intended purpose of modelling. As open-source tools like *OpenSim*, *STAPLE*, and AST continue to evolve, careful integration of participant-specific features allows the advancement of increased anatomical accuracy for simulation outputs in musculoskeletal modelling.

References

Alkjær, T., Smale, K., Flaxman, T., Marker, I., Simonsen, E., Benoit, D., Williams, J. (2020). Forward lunge before and after anterior cruciate ligament reconstruction: Faster movement but unchanged knee joint biomechanics. *PLOS* ONE, 15(11), e0242531. https://doi.org/10.1371/journal.pone.0242531.

Amberg, B., Romdhani, S., Vetter, T. (2007). Optimal step nonrigid ICP algorithms for surface registration. *In IEEE Conference on Computer Vision and Pattern Recognition,* 1-8. https://doi.org/10.1109/CVPR.2007.383165

Arnold, E., Ward, S., Lieber, R., Delp, S. (2010). A model of the lower limb for analysis of human movement. *Annals of Biomedical Engineering, 38*, 269-279. https://doi.org/10.1007/s10439-009-9852-5

Benoit, D.L., Ramsey, D.K., Lamontagne, M., Xu, L., Wretenberg, P., Renström, P. (2007). In vivo knee kinematics during gait reveals new rotation profiles and smaller translations. *Clinical Orthopaedics and Related Research, 454*, 81-8. https:/doi.org/10.1097/BLO.0b013e31802dc4d0.

Besl, P., McKay, N. (1992). A method for registration of 3-D shapes. *IEEE Transactions on Pattern Analysis and Machine Intelligence, 14*(2), 239-256.

Bradsell, H., Frank, R. (2022). Anterior cruciate ligament injury prevention. *Annals of Joint*, *7*. https://doi.org/10.21037/aoj-2020-01.

Brown, B., Rusinkiewicz, S. (2004). Non-rigid range-scan alignment using thin-plate splines*. In IEEE Proceedings of the 2nd International Symposium on 3D Data Processing, Visualization and Transmission*, 753-760. https://doi.org/10.1109/TDPVT.2004.1335392

Buford, W., Ivey, F., Malone, J., Patterson, R., Peare, G., Nguyen, D., Stewart, A. (1997). Muscle balance at the knee – Moment arms for the normal knee and the ACL-minus knee. *IEEE Transactions on Rehabilitation Engineering, 5*, 367-379.

Cabuk, H., Cabuk, F. (2016). Mechanoreceptors of the ligaments and tendons around the knee. *Clinical Anatomy, 29*(6), 789-795. https://doi.org/10.1002/ca.22743.

Carmen, L., Besier, T., Rooks, N., Choisne, J. (2024). An articulated shape model to predict paediatric lower limb bone geometry using sparse landmarks. *Journal of Biomechanics, 172*, 112211. https://doi.org/10.1016/j.jbiomech.2024.2024.112211.

Catelli, D., Wesseling, M., Jonkers, I., Lamontagne, M. (2019). A musculoskeletal model customized for squatting task. *Computer Methods in Biomechanics and Biomedical Engineering, 22*(1), 21-24. https://doi.org/10.1080/10255842.2018.1523396.

Cereatti, A., Bonci, T., Akbarshahi, M., Aminian, K., Barré, A., Begon, M., Benoit, D.L., Charbonnier, C., Dal Maso, F., Fantozzi, S., Lin, C., Lu, T., Pandy, M.G., Stagni, R., van den Bogert, A.J., Camomilla, V. (2017). Standardization proposal of soft tissue artefact description for data sharing in human motion measurements. *Journal of Biomechanics, 62,* 5-13. https://doi.org/10.1016/j.jbiomech.2017.02.004.

Charles, J., Fu, F., Anderst, W. (2021). Predictions of anterior cruciate ligament dynamics from subject-specific musculoskeletal models and dynamic biplane radiography. *Journal of Biomechanical Engineering, 143*(3), 031006. https://doi.org/10.1115/1.4048710.

Comfort, P., Jones, P., Smith, L., & Herrington, L. (2015). Joint kinetics and kinematics during common lower limb rehabilitation exercises. *Journal of Athletic Training, 50*(10), 1011-1018. https://doi.org/10.4085/1062-6050-50.10.03.

Conconi, M., Sancisi, N., Parenti-Castelli, V. (2018). Subject-specific model of knee natural motion: A non-invasive approach. In *Advances in Robot Kinematics by Springer International Publishing*, 255-264.

Conconi, M., De Carli, F., Berni, M., Sancisi, N., Parenti-Castelli, V., Monetti, G. (2023). In-vivo quantification of knee deep-flexion in physiological loading condition through dynamic MRI. *Advanced Imaging in Orthopedic Biomechanics, 13*(1), 629. https:/doi.org/10.3390/app13010629.

Deeley, M.; Chen, A.; Datteri, R.; Noble, J.; Cmelak, A.; Donnelly, E.; Malcolm, A.; Moretti, L.; Jaboin, J.; Niermann, K.; et al. (2011). Comparison of manual and automatic segmentation methods for brain structures in the presence of space-occupying lesions: a multi-expert study. *Physics in Medicine and Biology*, *56*, 4557–4577. https://doi.org/10.1088/0031-9155/56/14/017.

Delp, S., Maloney, W. (1993). Effects of hip center location on the moment-generating capacity of the muscles. *Journal of Biomechanics, 26*(4), 485-499. https://doi.org/10.1016/0021-9290(93)90011-3.

D'Lima, D., Patil, S., Steklov, N., Chien, S., Colwell, C. (2007). In vivo knee moments and shear after total knee arthroplasty. *Journal of Biomechanics, 40*, S11-S17. https://doi.org/10.1016/j.jbiomech.2007.03.004.

Escamilla, R., Macleod, T., Wilk, K., Paulos, L., Andrews, J. (2012). Anterior cruciate ligament strain and tensile forces for weight-bearing and non-weight-bearing exercises: a guide to exercise selection. *The Journal of Orthopaedic and Sports Physical Therapy, 42*(3), 208-220. https://doi.org/10.2519/jospt.2012.3768.

Fiederer, L., Alwanni, H., Völker, M., Schnell, O., Beck, J., Ball, T. (2019). A research framework for virtual reality neurosurgery based on open-source tools. *IEEE Transactions on Biomedical Engineering, 66*, 2120-2132. https://doi.org/10.1109/TBME.2019.2901523.

Gupton, M., Imonugo, O., Black, A., Launico, M., Terreberry, R. (2022). Anatomy, bony pelvis and lower limb, knee. *StatsPearls Publishing*, Chapter 1.

Handsfield, G., Meyer, C., Hart, J., Abel, M., Blemker, S. (2014). Relationships of 35 lower limb muscles to height and body mass quantifed using MRI. *Journal of Biomechanics, 47*(3), 631-638. https://doi.org/10.1016/j/jbiomech.2013.12.002

Hornsey, R., Hibbard, P. (2024). Current perceptions of virtual reality technology. *Applied Sci*ences, *14*, 4222. https://doi.org/10.3390/app14104222.

Johnston, A., Rae, J., Ariotti, N., Bailey, B., Lilja, A., Webb, R., Ferguson, C., Maher, S., Davis, T., Webb, R., McGhee, J., Parton, R. (2018). Journey to the centre of the cell: Virtual reality immersion into scientific data. *Traffic, 19*(2), 105-110. https://doi.org/10.1111/tra.12538.

Kai, S., Sato, T., Koga, Y., Omori, G., Kobayashi, K., Sakamoto, M., Tanabe, Y. (2014). Automatic construction of an anatomical coordinate system for three-dimensional bone models of the lower extremities – Pelvis, femur and tibia. *Journal of Biomechanics, 47*, 1229-1233. https://doi.org/10.1016/j.jbiomech.2013.12.013.

Kainz, H., Wesseling, M., Jonkers, I. (2021). Generic scaled versus subject-specific models for the calculation of musculoskeletal loading in cerebral palsy gait: Effect of personalized musculoskeletal geometry outweighs the effect of personalized neural control. *Clinical Biomechanics, 87*, 105402. https://doi.org/10.1016/j.clinbiomech.2021.105402.

Kim, Y., Jung, Y., Choi, W., Lee, K., Koo, S. (2018). Similarities and differences between musculoskeletal simulations of *OpenSim* and AnyBody modeling system. Journal of Mechanical Science and Technology, 32, 6037-6044. https://doi.org/10.1007/s12206-018-1154-0.

Kocabey, Y., Tetik, O., Isbell, W., Atay, A., Johnson, D. (2004). The value of clinical examination versus magnetic resonance imaging in diagnosis of meniscal tears and anterior cruciate ligament rupture. *Arthroscopy: The Journal of Arthroscopy and Related Surgery, 20*(7), 696-700. https://doi.org/10.1016/j.arthro.2004.06.008.

Konishi, Y., Fukubayashi, T., Takeshita, D. (2002). Possible mechanism of quadriceps femoris weakness in patients with ruptured anterior cruciate ligament. *Medicine & Science in Sports & Exercise, 34*(9), 1414-1418. https://doi.org/10.1097/00005768-200209000-00003.

Krogsgaard, M., Fischer-Rasmussen, T., Dyhre-Poulsen, P. (2011). Absence of sensory function in the reconstructed anterior cruciate ligament. *Journal of Electromyography and Kinesiology, 21*(1), 82-86. https://doi.org/10.1016/j.jelekin.2010.09.012.

Kundu, B., Yang, Z., Simon, R., Linte, C. (2024). Comparative analysis of non-rigid registration techniques for liver surface registration. *Proceedings of SPIE the International Society of Optical Engineering*, 12928, 129282B. https://doi.org/10.1117/12.3008594

Kway, Y., Thirumurugan, K., Tint, M., Michael, N., Shek, L., Yap, F., Tan, K., Godfrey, K., Chong, Y., Fortier, M., et al. (2021). Automated segmentation of visceral, deep subcutaneous, and superficial subcutaneous adipose tissue volumes in MRI of neonates and young children. *Radiology: Artificial Intelligence, 3*, e200140. https://doi.org/10.1148/ryai.2021200140.

Lai, A., Arnold, A., Wakeling, J. (2017). Why are antagonist muscles co-activated in my simulation? A musculoskeletal model for analyzing human locomotor task. *Annals of Biomedical Engineering, 45*(12), 2762-2774. https://doi.org/10.1007/s10439-017-1920-7.

LaPrade, R., Morgan, P., Wentorf, F., Johansen, S., Engebretsen, L. (2007). The anatomy of the posterior aspect of the knee: An anatomic study. *The Journal of Bone & Joint Surgery, 89*(4), 758-764. https://doi.org/102106/JBJS.F.00120.

Leardini A, Chiari L, Della Croce U, Cappozzo A. (2005). Human movement analysis using stereophotogrammetry. Part 3. Soft tissue artifact assessment and compensation. *Gait Posture, 21*(2), 212-25. https://doi.org/10.1016/j.gaitpost.2004.05.002.

Li, G., DeFrate, L., Rubash, H., Gill, T. (2005). In vivo kinematics of the ACL during weight-bearing knee flexion. *Journal of Orthopaedic Research, 23*(2), 340-344. https://doi.org/10.1016/j.orthres.2004.08.006.

Liimatainen, K., Latonen, L., Valkonen, M., Kartasalo, K., Ruusuvuori, P. (2021). Virtual reality for 3D histology: multi-scale visualization of organs with interactive feature exploration. *BMC Cancer, 21*(1), 1220. https://doi.org/10.1186/s12885-021-08964-0.

Malus, J., Skypala, J., Silvernail, J., Uchytil, J., Hamill, J., Barot, T., Jandacka, D. (2021). Marker placement reliability and objectivity for biomechanical cohort study: Healthy aging in industrial environment (HAIE- Program 4). *Sensors, 21*(5), 1830. https://doi.org/10.3390/s21051830.

MAP Client Team. (2024). *MAP client* documentation. Retrieved from: https://*MAP*client.readthedocs.io/

Marieswaren, M., Sikidar, A., Goel, A., Joshi, D., Kalyanasundaram, D. (2018). An extended *OpenSim* knee model for analysis of strains of connective tissues. *Biomedical Engineering OnLine*, 17(42). https://doi.org/10.1186/s12938-018-0474-8.

Martelli, S., Valente, G., Viceconti, M., Taddei, F. (2015). Sensitivity of a subject-specific musculoskeletal model to the uncertainties on the joint axes location. *Computer Methods in Biomechanics and Biomedical Engineering, 18*(14), 1555-1563. https://doi.org/10.1080/10255842.2014.930134.

Masouros, S., Bull, A., Amis, A. (2010). Biomechanics of the knee joint. *Orthopaedics and Trauma, 24*(2), 84-91. https://doi.org/10.1016/j.mporth.2010.03.005

Modenese, L., Montefiori, E., Wang, A., Wesarg, S., Viceconti, M., Mazza, C. (2018). Investigation of the dependence of joint contact forces on musculotendon parameters using a codified workflow for image-based modeling. *Journal of Biomechanics, 17*(73), 108-118. https://doi.org/j.jbiomech.2018.03.039.

Modenese, L., Renault, J.-B. (2021). Automatic generation of personalized skeletal models of the lower limb from three-dimensional bone geometries. *Journal of Biomechanics, 116*, 110186. https://doi.org/10.1016/j.jbiomech.2020.110186.

Myronenko, A., Song, X. (2010). Point set registration: Coherent point drift. *IEEE Transactions on Pattern Analysis and Machine Intelligence, 32*(12), 2262-2275.

Neumann, D. (2001). Kinesiology of the musculoskeletal system: Foundations for rehabilitation. (2nd ed.). *Mosby Elsevier*, Chapter 13, 520-573.

Nolte, D., Tsang, C., Dabnichki, P., Bull, A. (2016). Reconstruction of lower limb bone geometry using statistical shape and appearance models. *Medical Engineering & Physics, 38*(6), 593-602. https://doi.org/10.1016/j.medengphy.2016.03.002.

Nomura, E., Inoue, M., Osada, N. (2005). Anatomical analysis of the medial patellofemoral ligament of the knee, especially the femoral attachment. *Knee Surgery, Sports Traumatology, Arthroscopy, 13*, 510-515. https://doi.org/10.1007/s00167-004-0607-4.

Ohori, T., Mae, T., Shino, K., Tachibana, Y., Fujie, H., Yoshikawa, H., Nakata, K. (2017). Varus-valgus instability in the anterior-cruciate ligament-deficient knee: effect of posterior tibial load. *Journal of Experimental Orthopaedics*, *4*(24). https://doi.org/10.1186/s40634-017-0087-3.

OpenSim. (2019). Inverse Kinematics. SimTK Confluence. https://*OpenSim*confluence.atlassian.net/wiki/spaces/*OpenSim*/pages/53090037/Inverse+Kinematics

Pinskerova, V., Vavrik, P. (2020). Knee anatomy and biomechanics and its relevance to knee replacement. (1st ed.). *Springer International Publishing*, Chapter 14, 159-168. https://doi.org/ 10.1007/978-3-030-24243-5_14

Preukschas, A., Wise, P., Bettscheider, L., Pfeiffer, M., Wagner, M., Huber, M., Golriz, M., Fischer, L., Mehrabi, A., Rossler, F., Speidel, S., Hackert, T., Muller-Stich, B., Nikel, F., Kenngott, H. (2024). Comparing a virtual reality head mounted display to on screen three-dimensional visualization and two-dimensional computed tomography for training in decision making in hepatic surgery: a randomized controlled study. *Surgical Endoscopy, 38*(4), 2483-2496. https://doi.org/10.1007/s00464-023-09989-9.

Princelle, D., Davico, G., Viceconti, M. (2023). Comparative validation of two participant-specific modeling pipelines for predicting knee joint forces during level walking. *Journal of Biomechanics, 159*, 111758. https://doi.org/10.1016/j.jbiomech.2023.111758.

Rajagopal, A., Dembia, C., DeMers, M., Delp, D., Hicks, J., Delp, S. (2016). Full-body musculoskeletal model for muscle-driven simulation of human gait. *IEEE Transactions on Biomedical Engineering, 63*(10), 2068-2079. https://doi.org/ 10.1109/TBME.2016.2586891.

Renault, J., Aüllo-Rasser, G., Donnez, M., Parratte, S., Chabrand, P. (2018). Articular-surface-based automatic anaomtical coordinate systems for the knee bones. *Journal of Biomechanics, 80*, 171-178. https://doi.org//10.1016/j.jbiomech.2018.08.028.

Sartoretti, E., Sartoretti, T., Schwenk, Á., Alfieri, A., Czell, D., Wyss, M., Wildi, L., Binkert, C., Sartoretti-Shefer, S. (2022). High-resolution 3D versus standard-resolution 2D T2-weighted turbo spin echo MRI for assessment of lumbar nerve root compromise. *Journal of Tomography, 8*(1), 257-266. https://doi.org/10.3390/tomography8010020.

Satava RM, Jones SB. (1998). Current and future applications of virtual reality for medicine. *Proceedings of the IEEE, 86(*3), 484-489. https://doi.org/10.1109/5.662875.

Scheys, L., Van Campenhout, A., Spaepen, A., Suetens, P., Jonkers, I. (2008). Personalized MR-based musculoskeletal models compared to rescaled generic models in the presence of increased femoral anteversion: effect on hip moment arm lengths. *Gait Posture, 28*(3), 358-365. https://doi.org/10.1016/j.gaitpost.2008.05.002.

Seth, A., Sherman, M., Reinbolt, J., Delp, S. (2011). *OpenSim*: a musculoskeletal modeling and simulation framework for in silico investigations and exchange. *Procedia IUTAM, 2*, 212-232. https://doi.org/10.1016/j.piutam.2011.04.021.

Seth, A., Hicks, J., Uchida, T., Habib, A., Dembia, C., Dunne, J., Ong, C., DeMers, M., *Rajagopal*, A., Millard, M., Hamner, S., Arnold, E., Yong, J., Lakshmikanth, S., Sherman, M., Ku, J., Delp, S. (2018). *OpenSim*: Simulating

musculoskeletal dynamics and neuromuscular control to study human and animal movement. *PLoS Computational Biology, 14*(7), e1006223. https://doi.org/10.1371/journal.pcbi.1006223.

Smale, K., Conconi, M., Sancisi, N., Krogsgaard, M., Alkjaer, T., Parenti-Castelli, V., Benoit, D. (2019). Effect of implementing magnetic resonance imaging for participant-specific *OpenSim* models on lower-body kinematics and knee ligament lengths. *Journal of Biomechanics, 83*, 9-15. https://doi.org/10.1016/j.jbiomech.2018.11.016.

Smith, L., Nachtrab, J., LaCour, M., Cates, H., Freeman, M., Komistek, R. (2021). In vivo knee kinematics: How important are the roles of femoral geometry and the cruciate ligaments?. Journal of Arthroplasty, 36, 1445-1454. https://doi.org/10.1016/j.arth.2020.10.020.

Thelen, D. (2003). Adjustment of muscle mechanics model parameters to simulate dynamic contractions in older adults. *Journal of Biomechanical Engineering, 125*(1), 70-77. https://doi.org/10.1115/1.1531112

Vaienti, E., Scita, G., Ceccarelli, F., & Pogliacomi, F. (2017). Understanding the human knee and its relationship to total knee replacement. *Acta Biomedica, 88*(2), 6-16. https://doi.org/10.23750/abm.v88i2-S.6507

Valente, G., Crimi, G., Vanella, N., Schileo, E., Taddei, F. (2017). *nmsBuilder*: Freeware to create subject-specific musculoskeletal models for *OpenSim*. *Computer Methods and Programs in Biomedicine, 152*, 85-92. https://doi.org/10.1016/j.cmpb.2017.09.012.

Valente, G., Pitto, L., Testi, D., Seth, A., Delp, S., Stagni, R., Viceconti, M., Taddei, F. (2014). Are subject-specific musculoskeletal models robust to the uncertainties in parameter identification?. *PLoS One, 9*(11), e112625. https://doi.org/10.1371/journal.pone.0112625.

Warren, C. (2022). Development and application of congruence-based knee model in anterior cruciate ligament injured adolescents. Master Thesis, University of Ottawa.

Weiss, J., Gardiner, J. (2001). Computational modeling of ligament mechanics. *Critical Reviews in Biomedical Engineering, 29*(3), 303-371. https://doi.org/10.1615/critrevbiomedeng.v29.i3.20.

Woo, S., Abramowitch, S., Kilger, R., Liang, R. (2006). Biomechanics of knee ligaments: injury, healing, and repair. *Journal of Biomechanics, 39*(1), 1-20. https://doi.org/10.1016/j.jbiomech.2004.10.025.

Yang, L. (2020). Theoretical and numerical analysis of anterior cruciate ligament injury and its prevention. *Global Journal of Engineering Science and Researches, 20*(1), 46. https://doi.org/10.34257/GJREJVOL20IS1PG43.

Zhang, J., Besier, T. (2016). Accuracy of femur reconstruction from sparse geometric data using a statistical shape model. *Computer Methods in Biomechanics and Biomedical Engineering, 20(*5), 1-11. https://doi.org/10.1080/10255842.2016.1263301.

Zimny, M., Wink, C. (1991). Neuroreceptors in the tissues of the knee joint. Journal of Electromyography and Kinesiology, 1(3), 148-157. https:/doi.org/10.1016/1050-6411(91)90031-Y.

Appendix A

(A.1.1)

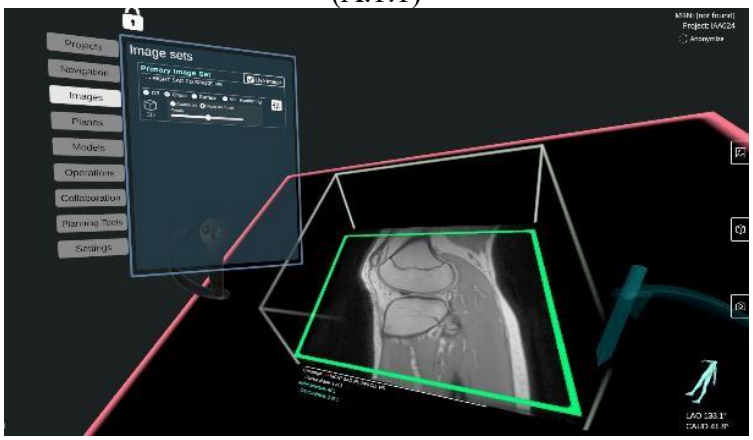

(B.1.1)

(A.2)

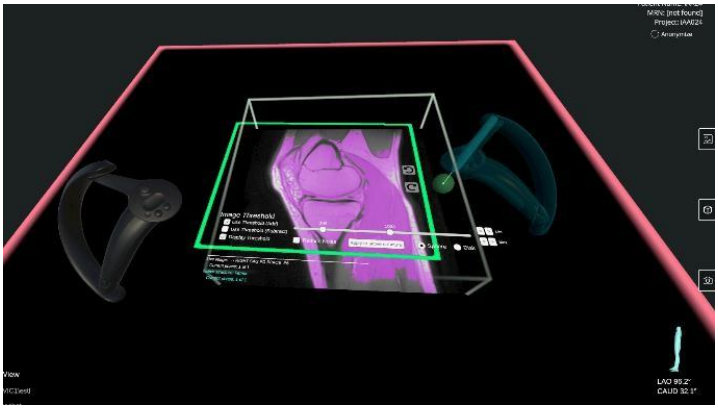

(B.2)

(A.3)

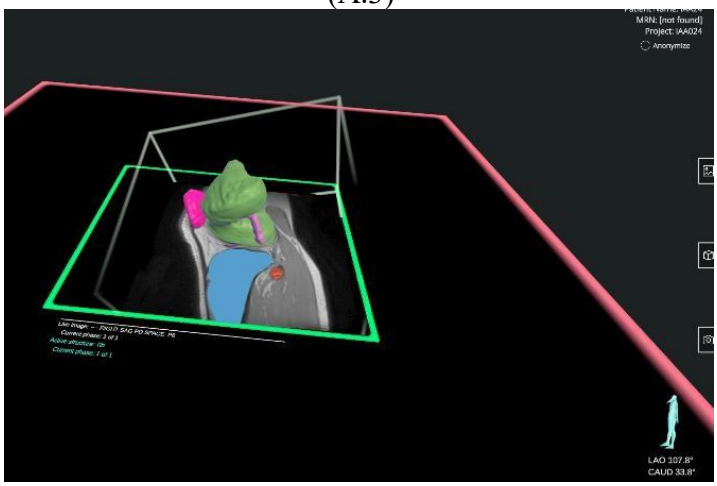

(B.3)

Figure A.1: Segmentation process compared between MITK (A.1.1, A.2, A.3) and Elucis (B.1.1, B.2, B.3). Highlighting differences in views and operations between importing images, determining object of interest, and creating 3D geometries from the masks through image frames. (A.1.1 v. B.1) Shows difference post-import of the high-resolution volumetric dataset (MRI). (A.2 v. B.2) Highlights opposing views to assess image sets by creating masks on objects of interest. (A.3 v. B.3) Varying software views when individual object masks have created digital models which are being smoothed and verified for accuracy.

Appendix B

Table B.1: MRI acquisition protocol for participants with knee imaging. Parameters are shown for GE 1.5T and Siemens 3T scanners both acquired using sagittal proton density Cube sequences.

Imaging Tag	**1.5 T GE** **(n = 24)**	**3 T Siemens** **(n = 9)**
Repetition Time (TR [ms])	2000	1400
Echo Time (TE [ms])	20	17
Flip Angle	90	160
Field of View	90 x 90	160 x 160
In plane Resolution	288 x 288	320 x 320
Bandwidth	244.141	~390

Appendix C

The study was approved by the CHILDREN'S HOSPITAL OF EASTERN ONTARIO (17/74X), and the UNIVERSITY OF OTTAWA (H091710).

Université d'Ottawa
Bureau d'éthique et d'intégrité de la recherche

University of Ottawa
Office of Research Ethics and Integrity

CERTIFICAT D'APPROBATION ÉTHIQUE | CERTIFICATE OF ETHICS APPROVAL

Numéro du dossier / Ethics File Number	H-12-23-9897
Titre du projet / Project Title	Knee joint function pre- and post-surgery among paediatric patients: a longitudinal perspective
Type de projet / Project Type	Recherche de professeur / Professor's research project
Statut du projet / Project Status	Approuvé / Approved
Date d'approbation (jj/mm/aaaa) / Approval Date (dd/mm/yyyy)	29/01/2024
Date d'expiration (jj/mm/aaaa) / Expiry Date (dd/mm/yyyy)	15/05/2024

Équipe de recherche / Research Team

Chercheur / Researcher	Affiliation	Role
Daniel BENOIT	École des sciences de la réadaptation / School of Rehabilitation Sciences	Chercheur Principal / Principal Investigator
Sasha CARSEN	Département de chirurgie / Department of Surgery	Co-chercheur / Co-investigator
Holly LIVOCK	The Children's Hospital of Eastern Ontario	Coordonnateur de recherche / Research Coordinator
Elese ST LOUIS	Département de génie mécanique / Department of Mechanical Engineering	Étudiant-chercheur / Student-researcher
Teresa FLAXMAN	Ottawa Hospital Research Institute	Collaborateur / Collaborator

Conditions spéciales ou commentaires / Special conditions or comments

The uOttawa expiry date of May 15th, 2024 is set in accordance with the ethics certificate from the CHEO REB.

Université d'Ottawa
Bureau d'éthique et d'intégrité de la recherche

University of Ottawa
Office of Research Ethics and Integrity

Le Comité d'éthique de la recherche (CÉR) de l'Université d'Ottawa, opérant conformément à l'*Énoncé de politique des Trois conseils* (2014) et toutes autres lois et tous règlements applicables, a examiné et approuvé la demande d'éthique du projet de recherche ci-nommé.

L'approbation est valide pour la durée indiquée plus haut et est sujette aux conditions énumérées dans la section intitulée "Conditions Spéciales ou Commentaires". Le formulaire « Renouvellement ou Fermeture de Projet » doit être complété quatre semaines avant la date d'échéance indiquée ci-haut afin de demander un renouvellement de cette approbation éthique ou afin de fermer le dossier.

Toutes modifications apportées au projet doivent être approuvées par le CÉR avant leur mise en place, sauf si le participant doit être retiré en raison d'un danger immédiat ou s'il s'agit d'un changement ayant trait à des éléments administratifs ou logistiques du projet. Les chercheurs doivent aviser le CÉR dans les plus brefs délais de tout changement pouvant augmenter le niveau de risque aux participants ou pouvant affecter considérablement le déroulement du projet, rapporter tout évènement imprévu ou indésirable et soumettre toute nouvelle information pouvant nuire à la conduite du projet ou à la sécurité des participants.

The University of Ottawa Research Ethics Board, which operates in accordance with the *Tri-Council Policy Statement* (2014) and other applicable laws and regulations, has examined and approved the ethics application for the above-named research project.

Ethics approval is valid for the period indicated above and is subject to the conditions listed in the section entitled "Special Conditions or Comments". The "Renewal/Project Closure" form must be completedfour weeks before the above-referenced expiry date to request a renewal of this ethics approval or closure of the file.

Any changes made to the project must be approved by the REB before being implemented, except when necessary to remove participants from immediate endangerment or when the modification(s) only pertain to administrative or logistical components of the project. Investigators must also promptly alert the REB of any changes that increase the risk to participant(s), any changes that considerably affect the conduct of the project, all unanticipated and harmful events that occur, and new information that may negatively affect the conduct of the project or the safety of the participant(s).

Riana MARCOTTE
Responsable d'éthique en recherche / Protocol Officer
Pour/For **Daniel LAGAREC** Président(e) du/ Chair of the **Comité d'éthique de la recherche en sciences de la santé et sciences / Health Sciences and Sciences Research Ethics Board**

Université d'Ottawa
Bureau d'éthique et d'intégrité de la recherche

University of Ottawa
Office of Research Ethics and Integrity

Lettre d'approbation administrative | Letter of administrative approval

Numéro de dossier / Ethics File Number	H-10-22-8524
Titre du projet / Project Title	Comparison of MRI Segmentation Software in Anterior Cruciate Ligament (ACL) Injured Pediatric Participants
Type de projet / Project Type	Recherche de professeur / Professor's research project
CÉR primaire / Primary REB	The Ottawa Hospital (OHRI) and CHEO
Statut du projet / Project Status	Approuvé / Approved
Date d'approbation (jj/mm/aaaa) / Approval Date (dd/mm/yyyy)	04/11/2022
Date d'expiration (jj/mm/aaaa) / Expiry Date (dd/mm/yyyy)	15/09/2023

Équipe de recherche / Research Team

Chercheur / Researcher	Affiliation	Role
Daniel BENOIT	École des sciences de la réadaptation / School of Rehabilitation Sciences	Chercheur Principal / Principal Investigator
Teresa FLAXMAN		Co-chercheur principal / Co-principal investigator
Elese ST LOUIS	Département de génie mécanique / Department of Mechanical Engineering	Étudiant-chercheur / Student-researcher
Holly LIVOCK	The Children's Hospital of Eastern Ontario	Coordonnateur de recherche / Research Coordinator

Conditions spéciales ou commentaires / Special conditions or comments:

CTO Project ID: 4160

Université d'Ottawa
Bureau d'éthique et d'intégrité de la recherche

University of Ottawa
Office of Research Ethics and Integrity

L'Université d'Ottawa a signé une Entente, conforme aux exigences de la plus récente version de l'EPTC et tout autre règlement ou législation applicable, permettant au CÉR ci-haut nommé d'être désigné comme CÉR primaire pour les projets de recherche où

1) les activités principales de recherche sont menées sous l'autorité ou sous les auspices de l'établissement lié au CÉR primaire et

2) Une partie du projet est également réalisé sous l'autorité ou sous les auspices de l'Université d'Ottawa.

Cette lettre confirme que l'Université d'Ottawa a autorisé que le CÉR primaire soit le CÉR officiel pour l'évaluation et la supervision de ce projet de recherche. Ceci n'est pas une approbation éthique.

Afin de nous aider à garder votre dossier à jour, veuillez soumettre une copie de toutes demandes de modification, renouvellement d'approbation éthique etc. soumis à et approuvé par le CÉR primaire dès qu'elles sont disponibles.

Cette approbation administrative est valide pour la durée indiquée ci-haut et est sujette aux conditions énumérées dans la section intitulée « Conditions spéciales ou commentaires ».

The University of Ottawa has signed an Agreement, compliant with current TCPS guidelines and any other applicable guidelines or legislation regarding multisite review, allowing the REB named above to serve as Board of Record (BoR) for research projects where

1) the main research activities are conducted within the auspices or jurisdiction of the BoR's institution and

2) parts of the project are also conducted under the jurisdiction or auspices of the University of Ottawa.

This letter confirms that the University of Ottawa has authorized the REB named above to serve as Board of Record for the review and oversight of this research project. This is not an REB approval.

In order to help us keep your file up to date, please submit a copy of all amendment requests, project renewals or any other changes submitted to and approved by the BoR, as they become available.

Administrative approval is valid for the period indicated above and is subject to the conditions listed in the section entitled «Special conditions or comments».

Catherine PAQUET
Directeur / Director
Pour/For **Daniel LAGAREC** Président(e) du/ Chair of the **Comité d'éthique de la recherche en sciences de la santé et sciences / Health Sciences and Sciences Research Ethics Board**